CHALMERS UNIVERSITY OF TECHNOLOGY
Gothenburg, Sweden
www.chalmers.se

LICENTIATE THESIS

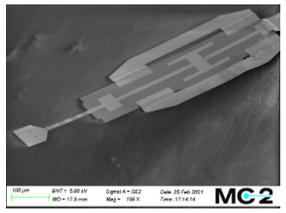
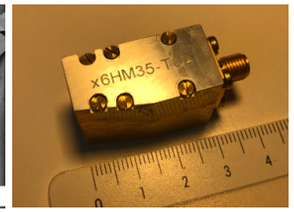

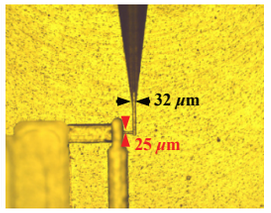

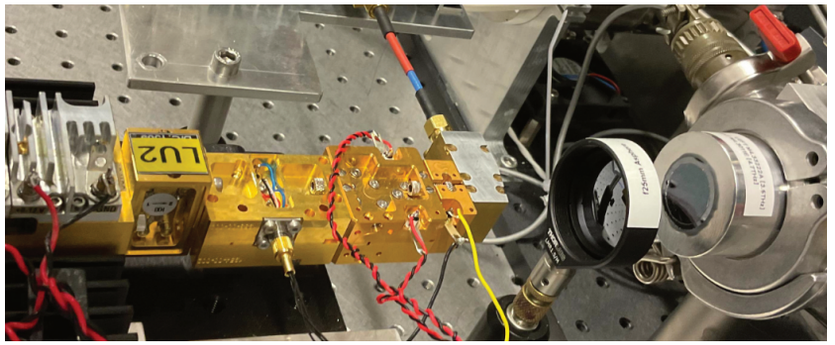

Design and characterisation of terahertz Schottky diode harmonic mixers

DIVYA JAYASANKAR

DEPARTMENT OF MICROTECHNOLOGY AND NANOSCIENCE - MC2
CHALMERS UNIVERSITY OF TECHNOLOGY
Gothenburg, Sweden 2021
www.chalmers.se

DIVYA JAYASANKAR • Design and characterisation of terahertz Schottky diode harmonic mixers • 2021

CHALMERS
UNIVERSITY OF TECHNOLOGY

THESIS FOR THE DEGREE OF LICENTIATE OF ENGINEERING

Design and characterisation of terahertz Schottky diode harmonic mixers

Divya Jayasankar

Terahertz and Millimetre wave Laboratory
Department of Microtechnology and Nanoscience - MC2
Chalmers University of Technology
Gothenburg, Sweden, 2021

Design and characterisation of terahertz Schottky diode harmonic mixers

Divya Jayasankar

ORCID: 0000-0002-5726-327X

Technical Report No. MC2-445
ISSN 1652-0769

This thesis has been prepared using LaTeX.
Terahertz and Millimetre wave Laboratory
Department of Microscience and Nanotechnology - MC2
Chalmers University of Technology
SE-412 96 Gothenburg, Sweden
Phone: +46 (0)31 772 1000
www.chalmers.se

Cover picture: Top from left to right: Scanned electron micrograph of the harmonic mixer integrated circuit defined on a 2-μm GaAs substrate. Photograph of the 3.5-THz, $\times$6-harmonic mixer block. Micrograph of the bottom E-plane split block showing the RF diagonal feedhorn integrated with the rectangular waveguide. Bottom: Photograph of the RF mixer characterisation setup at DLR, Berlin showing the 3.5-THz quantum-cascade laser, and harmonic mixer connected to a 600-GHz multiplier chain.

Printed by Chalmers Reproservice
Gothenburg, Sweden, November 2021

'If I have seen further it is by standing on the shoulders of giants' - Issac Newton

Abstract

Efficient, compact, and reliable terahertz frequency converters preferably operating at ambient temperature are crucial for stabilising far-infrared optical sources. This thesis focuses on the design and characterisation of terahertz Schottky diode harmonic mixers for frequency stabilisation of quantum-cascade lasers.

First, the influence of idler terminations on harmonic mixer performance and diode embedding impedance at radio and local oscillator frequencies was studied. Based on this, a 3.5-THz, $\times$6-harmonic mixer was designed. A planar, single-ended Schottky diode with a sub-μm contact area was realised on a 2-μm suspended GaAs substrate. The integrated mixer circuit was assembled in an E-plane split-block with the aid of beam leads. The Schottky diode anode pad was designed to act as a radio frequency E-plane probe and extended as a beamlead to provide dc ground, resulting in an electrically compact circuit. The design was validated by conducting a sensitivity analysis of critical parameters that are susceptible to fabrication tolerances. Two integrated circuits with Schottky contact areas of 0.11 and 0.14 μm^2 were assembled on mixer modules and dc/RF characterisation was carried out. Both harmonic mixers exhibited a conversion loss of about 60 dB at an intermediate frequency of 200 MHz. When evaluated in a phase-locked loop, it resulted in a signal-to-noise ratio of 40 dB, which was more than sufficient to phase lock the quantum-cascade lasers.

This work presents uncooled, efficient THz harmonic mixers for stabilising THz optical sources. It opens up many opportunities for building a THz heterodyne spectrometer with a high spectral resolution to detect gas species such as hydroxyl radical and atomic oxygen in the frequency range of 3-5 THz.

Keywords: Frequency converters, Frequency stabilisation, Harmonic mixers, Heterodyne receivers, Phase locking, Schottky diodes, Terahertz electronics.

List of Publications

This thesis is based on the following appended publications:

[A] **D. Jayasankar**, J. Stake and P. Sobis, "Effect of Idler Terminations on the Conversion Loss for THz Schottky Diode Harmonic Mixers," in proceedings of the *44th Int. Conf. on Infrared, Millimeter, and Terahertz waves (IRMMW-THz)*, Paris, Sep. 2019, pp. 1-2,DOI: 10.1109/IRMMW-THz.2019.8873938.

[B] **D. Jayasankar**, V. Drakinskiy, N. Rothbart, H. Richter, X Lü, L Schrottke, H T. Grahn, M. Wienold, H-W. Hübers, P. Sobis, and J. Stake, "A 3.5-THz, ×6-Harmonic, Single-Ended Schottky Diode Mixer for Frequency Stabilization of Quantum-Cascade Lasers," *IEEE Transactions on Terahertz Science and Technology*, vol. 11, no. 6, pp. 684-694, Nov. 2021, DOI: 10.1109/TTHZ.2021.3115730.

[C] **D. Jayasankar**, V. Drakinskiy, P. Sobis, and J. Stake, "Development of Supra-THz Schottky Diode Harmonic Mixers," in proceedings of the *46th Int. Conf. on Infrared, Millimeter, and Terahertz waves (IRMMW-THz)*, Chengdu, Sep. 2021, DOI: 10.1109/IRMMW-THz50926.2021.956.

Other publications that are not included as they are beyond the scope of this thesis:

[D] H. Richter, N. Rothbart, M. Wienold, X Lü, L Schrottke, H T. Grahn, **D. Jayasankar**, V. Drakinskiy, P. Sobis, J. Stake, and H-W. Hübers, "Phase Locking of 3.5-THz and 4.7-THz Quantum-Cascade Lasers Using a Schottky Diode Harmonic Mixer", in proceedings of the *46th Int. Conf. on Infrared, Millimeter, and Terahertz waves (IRMMW-THz)*, Chengdu, Sep. 2021, pp. 1–2, DOI:10.1109/IRMMW-THz50926.2021.9566876.

[E] **D. Jayasankar**, V. Drakinskiy, P. Sobis, and J. Stake, "Design and development of 3.5 THz Schottky-based fundamental mixer", in proceedings of the *2020 50th European Microwave Conference (EuMC)*, Utrecht, Jan. 2021, pp. 595-598, DOI: 10.23919/EuMC48046.2021.9338204.

[F] P. Sobis, V. Drakinskiy, **D. Jayasankar**, A. Hammar, M. Anderberg, A. Emrich, E. Saenz, and J. Stake, "4.7 THz GaAs Schottky diode receiver components", in proceedings of the *30th Int. Symp. on Space Terahertz Technology (ISSTT)*, Gothenburg, Apr. 2019, pp. 133.

[G] J. Vukusic, V. Drakinskiy, D. Heineråas, **D. Jayasankar**, T. Bryllert, V. Valenta, M. Geneviev, F. Martin, and J. Stake, "Reliability assessment of GaAs and InP THz mixers and frequency multipliers fabricated on 3" wafers", in proceedings of the *30th Int. Symp. on Space Terahertz Technology (ISSTT)*, Gothenburg, Apr. 2019, pp. 134.

Acknowledgments

Foremost, I would like to express my sincere gratitude to Prof. Jan Stake for his guidance and unwavering belief in me during the course of my master's and PhD studies. I am forever indebted to the supra-THz team members, Dr. Peter Sobis, Mr. Vladimir Drakinskiy, and Mr. Mats Myremark, for their remarkable expertise and for being my pillar of support. Thanks to Dr. Tomas Bryllert and Dr. Josip Vukusic for all the fruitful discussions. I am grateful to my examiner Prof. Christian Fager for his continued support. Special thanks to colleagues from the German Aerospace Center (DLR), Dr. Heiko Richter, Dr. Nick Rothbart, and Prof. Heinz-Wilhelm Hübers for their support and encouragement. My sincere gratitude to colleagues from the Paul-Drude Institute for Semiconductor Physics (PDI), Dr. Lutz Schrottke, Dr. Xiang Lü and Prof. Holger T. Grahn for their insightful comments and suggestions. Thanks to Dr. Nick Ridler, Mr. Steven Durant, and Dr. Jeffrey Hesler for all the discussions in the TEMMT project. My appreciation also goes to Dr. Karin Cedergren, Dr. Tobias Bergsten, Dr. Per Olof Hedekvist and colleagues from the Research Institutes of Sweden (RISE), Borås.

I appreciate the Ericsson research foundation for funding my research visit to Germany and the European Microwave Association (EuMA) for the internship award. This PhD was supported by the Swedish Foundation for strategic research (SSF). The mixer development was carried out in the GHz centre and financed by the European Space Agency (ESA) and the Swedish National Space Board (SNSB).

To incredible women in my life, Balasaraswathy Jayasankar, Jayashree S., Dr. Mayuri S. Rao, Sara Catteau, Debora Perlheden, and Dr. Irina Nefedova. Thanks for being the shoulder I can always depend on. Thanks to Fida, Sam, Niklas, Rasmus, Andreas, Calle, Ayron and Azega for making me feel at home. Thanks to colleagues Junjie, Yin, Jenny, Juan, Marlene and Anis for making this journey more fun and exciting. Last but not least, I would like to dedicate this thesis to my Amma and Appa for their love and support.

Divya Jayasankar
Göteborg, Nov. 2021

Acronyms

AM	Amplitude Modulation
Au	Gold
CAD	Computer Aided Design
Cr	Chromium
CVD	Chemical Vapour Deposition
CW	Continuous Wave
DC	Direct Current
DLR	Deutsches zentrum für Luft- und Raumfahrt
DSB	Double Side-Band
DUT	Device Under Test
EM	Electromagnetic
ESA	European Space Agency
FEM	Finite Element Method
FET	Field Effect Transistor
FIR	Far Infrared
GaAs	Gallium Arsenide
Ge	Germanium
HB	Harmonic Balance
HEB	Hot Electron Bolometer
Hz	Hertz
IC	Integrated Circuit

IF	Intermediate Frequency
IR	Infrared
LNA	Low Noise Amplifier
LO	Local Oscillator
LOCUS	Linking Observations of Climate, the Upper atmosphere and Space weather
MMIC	Microwave Monolithic Integrated Circuit
MLT	Mesosphere-Lower Thermosphere
MoM	Method of Moments
PDI	Paul-Drude-Institut für Festkörperelektronik
PLL	Phase Locked Loop
Pt	Platinum
QCL	Quantum-Cascade Laser
RF	Radio Frequency
S-parameter	Scattering parameter
SiO_2	Silicon dioxide
SSB	Single Side-Band
SOFIA	Stratospheric Observatory for Far-Infrared Astronomy
Ti	Titanium
TPX	Polymethylpentene
3-D	Three Dimension

Symbols

k_B	Boltzmann's constant
N_{buf}	Buffer layer doping concentration
Φ_B	Barrier height
ψ_{bi}	Built-in potential
E_c	Conduction band
L	Conversion loss
η	Diode ideality factor
w_d	Depletion width
Z_{IF}	Diode embedding impedance at IF
Z_{LO}	Diode embedding impedance at LO
Z_{RF}	Diode embedding impedance at RF
m_e	Effective electron mass
m_h	Effective hole mass
A^{**}	Effective Richardson's constant
σ_{buf}	Electrical conductivity of buffer layer
σ_{epi}	Electrical conductivity of epi-layer
χ_s	Electron affinity
q	Elementary charge
N_{epi}	Epi-layer doping concentration
V_F	Forward voltage
λ_g	Guide wavelength
C_j	Junction capacitance
μ_n	Low-field electron mobility
μ_p	Low-field hole mobility
μ_0	Magnetic permeability of free space
ϕ_m	Metal work function
L	Mixer conversion loss
ϵ_0	Permittivity of free space
h	Planck's constant
ϵ_r	Relative permittivity
V_R	Reverse voltage
S	Schottky contact area

E_g	Semiconductor bandgap
R_s	Series resistance
c	Speed of light in vacuum
δ_s	Skin depth
t_{epi}	Thickness of epi-layer
E_v	Valence band
λ	Wavelength
C_{j0}	Zero-bias junction capacitance

Constants

c	$2.9979 \times 10^{8}\,\text{m/s}$
h	$6.6260 \times 10^{-34}\,\text{m}^2\ \text{kg/s}$
k_B	$1.3806 \times 10^{-23}\,\text{m}^2\ \text{kg}\ \text{s}^{-2}\ \text{K}^{-1}$
μ_0	$4\pi \times 10^{-7}\,\text{H}\ \text{m}^{-1}$
ϵ_0	$8.8541 \times 10^{-12}\,\text{F}\ \text{m}^{-1}$
q	$1.6021 \times 10^{-19}\,\text{coulombs}$

Contents

CHAPTER 1

Introduction

Terahertz (THz) heterodyne spectroscopy is an invaluable tool to understand the physics, distribution profile, and concentration of molecular and atomic gas in space [1]–[4]. Studying the chemical composition of the Earth's atmosphere can provide valuable insights into global warming and climate change. In particular, detection of gas species such as atomic oxygen (OI) at 4.7 THz [5], [6], and hydroxyl radical (OH) at 3.5 THz in the mesosphere-lower thermosphere (MLT) regions can improve the climate and weather prediction models [7]–[9].

Despite its attractive scientific potential, THz is the least explored region in the electromagnetic spectrum due to the unavailability of sources. However, with the recent development of quantum-cascade lasers (QCLs), the realisation of THz heterodyne spectrometers has become feasible [10], [11]. QCLs can provide a few-mW of output power and operate in continuous-wave (CW) mode, thereby making it an ideal candidate as a local oscillator (LO) source for THz spectrometers [12]–[14]. However, they are sensitive to cryocooler vibrations, temperature, and bias current variations, leading to frequency drifts and instabilities. Hence, it is critical to stabilise the LO sources for resolving fine features in the gas emission spectra.

Many authors have reported phase-locking of a QCL, and a few of them are summarised here. In 2009, Rabanus *et al.* demonstrated phase locking of 1.5-THz QCL using a hot-electron bolometer (HEB) as well as employed the QCL as an LO source in a heterodyne experiment [15]. However, HEBs requires a cryocooler for their operation, and therefore, is not suitable for long lifetime space and airborne missions.

Frequency converters preferably operating at ambient temperatures are required to meet future earth observation missions scientific objectives and instrumentation requirements. Detectors based on Schottky diode technology are the workhorses behind high-altitude balloons and space-borne missions such as ODIN and Microwave Instrument for Rosetta Orbiter (MIRO) [16]–[18]. Schottky varactor diodes are employed as frequency multipliers in the LO chain that pumps the mixers are utilised in the Heterodyne Instrument for Far-Infrared (HIFI) instrument onboard of Herschel space observatory (HSO) [19], and Sub-millimetre Wave Instrument (SWI) in JUpiter ICy moons Explorer (JUICE) mission [20]. It offers a wide range of intermediate frequencies (IF), fast response time, and can work in ambient temperatures, thereby eliminating the need for cryocoolers [21]. In 2005, Betz *et al.* demonstrated phase-locking of a 3-THz QCL to a far-infrared gas laser using a corner cube mount GaAs Schottky diode mixer [22]. Erickson *et al.* [23] reported the first THz balanced Schottky diode mixer in 2009. Subsequently, Danylov *et al.* [24] demonstrated phase locking of a 2.32-THz QCL using a balanced-Schottky diode $\times$21-harmonic mixer, which exhibited a conversion loss of about 110 dB. Bulcha *et al.* has demonstrated phase locking of 2.5-THz QCL using a single-ended Schottky diode $\times$4-harmonic mixer which yielded 35 dB conversion loss [25]-[26]. Hence, it is desirable to have compact, efficient and reliable harmonic mixers operating above 3 THz, which can be utilised in frequency stabilisation of far-infrared optical sources.

This thesis presents the development of Schottky diode-based harmonic mixers operating above 3 THz for QCL frequency stabilisation. A detailed large-signal analysis of harmonic mixers with different idler terminations was carried out to improve the harmonic mixer's performance. [Paper A] presents the corresponding diode embedding impedances at RF and LO frequencies and the mixer conversion loss. Based on this theoretical evaluation, a 3D-electromagnetic (EM) model was implemented using a FEM solver (Ansys HFSS). The designed mixer circuits and blocks were fabricated at the Chalmers

University of Technology. A 600-GHz, ×64-cascaded active multiplier chain was used to pump the harmonic mixer. The QCL was grown and fabricated at Paul Drude Institute for solid-state electronics (PDI), Berlin. The RF mixer characterisation was carried out at the German Aerospace Center (DLR), Berlin and the results are summarised in [Paper B]. The discrepancy between the EM-simulation and measurements are discussed, and from this understanding, a design of 4.7-THz, ×8-harmonic mixer was carried out, and the preliminary simulation results are presented in [Paper C].

The thesis begins with an overview of Schottky diodes, diode I-V characteristics, estimation of diode series resistance and junction capacitance, heterodyne detectors and mixer theory. It is followed by Chapter 3 about the design of the 3.5-THz planar, single-ended Schottky diode ×6-harmonic mixer. Chapter 3 also concludes with a brief discussion of the integrated circuit and mixer block fabrication and mixer assembly. Finally, in Chapter 4, the dc/RF characterisation results are presented. The results show promising prospects for the availability of compact, uncooled, and efficient THz harmonic mixers, which opens up many opportunities for building future air/space-borne heterodyne receivers with a high spectral resolution.

CHAPTER 2

Theory

This chapter starts with a brief overview of the historical development and theory of Schottky diodes. The second part of this chapter is devoted to mixer theory, and a brief overview of few mixer topologies.

> "The Schottky-barrier diode is the cockroach of microwave technology: it is has been around since the beginning and is impossible to exterminate. Schottky-barrier diodes existed before any other microwave electronic devices and will be around long after all the others are gone [27]." - Stephen A. Maas

2.1 Schottky diode

Schottky diode is a two-terminal device composed of a metal-semiconductor (M-S) junction. Fig. 2.1 shows the symbol and cross-section of the Schottky diode. The first work on metal-semiconductor diodes was reported in 1874 by Ferdinand Braun, who observed the current rectification effect while probing a galena crystal (lead sulfide) with a metal wire [28]. Crystal detectors played an essential role in the development of wireless telegraphy, for which he was

awarded the Nobel prize in 1909 together with Marconi [29]. Around the same time, crystal detectors operating up to 60 GHz were developed by J.C. Bose [30]

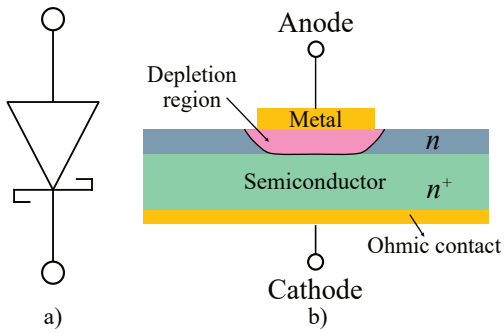

Figure 2.1: Schottky barrier diode a) Schottky diode symbol b) Cross section of the metal-semiconductor junction and the depletion region is indicated by dotted lines.

Walter H. Schottky [31] postulated the concept of depletion layer; majority charge carrier conduction over the barrier; the relation between the barrier height and work function of metal and semiconductor; image-force lowering effect [32]. A metal-semiconductor junction can act as a Schottky barrier depending upon the barrier height Φ_b, and it is given by,

$$\Phi_b = \phi_m - \chi_s \tag{2.1}$$

where ϕ_m is the metal-work function and χ_s is the electron affinity in the semiconductor [33]-[34]. Both n- or p-type semiconductors can be used to realise a Schottky diode. However, for high-frequency applications, n-doped GaAs is preferred due to high electron mobility and carrier velocity [35]. Typical metals used as an anode contact are chromium (Cr), titanium (Ti), platinum (Pt), and gold (Au). For n-type semiconductors, the most commonly used ohmic metal is gold-germanium (Au-Ge) [36].

Under thermal equilibrium conditions, a depletion region of width W_d is created due to the flow of electrons from the n-type semiconductor to the metal. Further transport of electrons is prevented due to the built-in potential (ψ_{bi}) created between the metal and semiconductor junction as shown in Fig. 2.2a.

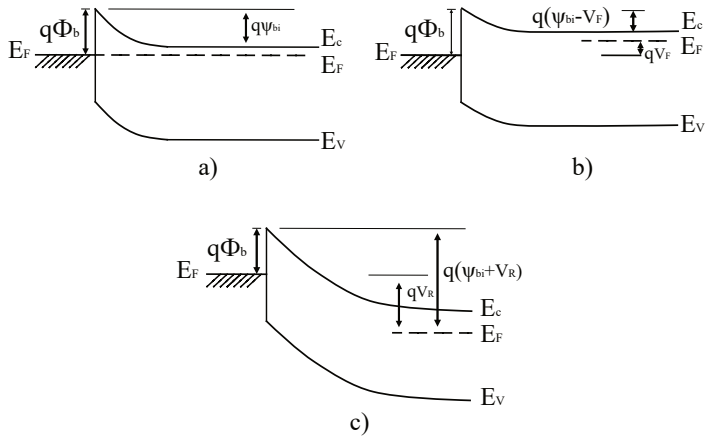

Figure 2.2: Energy band diagram of a metal and (n-type) semiconductor junction. (a) Thermal equilibrium, (b) Forward bias V_F, and (c) Reverse bias V_R.

An external voltage has to be applied across the diode, i.e., forward bias or reverse bias, to facilitate movement of majority carriers [37]. Depending upon the polarity of the applied voltage, the depletion width (W_d) of the space-charge region can be altered. Under forward bias condition see Fig. 2.2b, the diode operates in a voltage-controlled resistor mode, also known as a varistor. Resistive mixers are generally operated in the varistor mode. Under reverse bias condition as shown in Fig. 2.2c, it acts as a voltage-controlled capacitor, or varactor [38]. Schottky diodes are typically operated in varactor mode for highly efficient frequency multiplication applications [39]. Material properties of GaAs at room temperature is given in Table 2.1.

Table 2.1: GaAs material properties at 300 K [40]–[42]

Symbol	Description	Value
E_g	Bandgap energy	1.42 eV
ϵ_s	Relative permittivity	12.9
m_e^*	Effective electron mass	0.063
μ_n	Low-field electron mobility	9000 cm^2/V.s

2.1.1 Diode equivalent circuit

A quasi-static equivalent circuit model for a Schottky diode is as shown below in Fig. 2.3. It consists of three elements, a series resistance (R_s), a non-linear junction capacitance and a current source. With quasi-static assumption, all non-linear elements are assumed to change instantaneously when their control voltage varies. It allows representing the equivalent circuit of a solid-state device by lumped linear and non-linear elements.

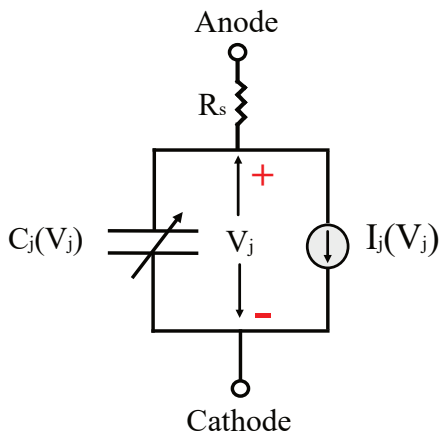

Figure 2.3: Quasi-static equivalent circuit model of a Schottky diode.

2.1.2 Current-voltage characteristic

The current flow in a Schottky diode is governed by the following carrier transport mechanisms: thermionic emission, tunnelling, and recombination of holes. For n-type semiconductors, current due to the minority charge carriers can be neglected. Schottky diodes that are realised using high-mobility semiconductors, such as GaAs, the majority carrier transportation is dominated by thermionic emission. Richardson was the first to explain the process of thermionic emission in vacuum tubes [43]. Later, Bethe proposed that it is also applicable to Schottky diodes [44]. Richardson's constant can be experimentally obtained by measuring the saturation current density as a function of temperature [45]. The current-voltage (I-V) characteristic of metal and n-type GaAs contact is given by

$$I_j(V_j) = I_s \left(exp(\frac{qV_j}{\eta k_B T}) - 1 \right) \tag{2.2}$$

where,

$$I_s = SA^{**}T^2 exp\left(\frac{-q\phi_b}{k_B T}\right) \tag{2.3}$$

$I_j(V_j)-$ Diode junction current,
I_s − Reverse saturation current,
V_j − Junction voltage,
$\eta-$ Ideality factor,
$S-$ Schottky contact area,
$A^{**}-$ Effective Richardson's constant [45],
$T-$ Absolute temperature,
ϕ_b- Barrier height,
$q-$ Elementary charge
k_B- Boltzmann's constant

For an ideal diode with conduction dominated by thermionic emission, the ideality factor η is equal to 1. However, an high epi-layer doping concentration can result in a narrow depletion width $W_d = \sqrt{\frac{2\epsilon_s \psi_{bi}}{qN_{\text{epi}}}}$ thereby causing the electrons to tunnel through the barrier which degrades the ideality factor [32].

2.1.3 Junction capacitance

The voltage-dependent junction charge and corresponding capacitance for a homogeneously doped diode can be derived using Poisson's equation [46].

The voltage-dependent depletion width is given by,

$$W_d = \sqrt{\frac{2\epsilon_s}{qN_{\text{epi}}}(\psi_{bi} - V)} \tag{2.4}$$

where ϵ_s is the relative permittivity of the semiconductor, N_{epi} is the epi-layer doping concentration, and V is the applied dc voltage across the diode.

The space charge Q_j is,

$$Q_j = SqN_{\text{epi}}W_d = S\sqrt{2q\epsilon_s N_{\text{epi}}(\psi_{bi} - V)} \tag{2.5}$$

and the junction capacitance is,

$$C_j \equiv \frac{\epsilon_s}{W_d} = S\sqrt{\frac{q\epsilon_s N_{\text{epi}}}{2(\psi_{bi} - V)}} \tag{2.6}$$

When the voltage applied across the diode is varied, the depletion width W_d will also vary as a function of the junction voltage. The zero-bias junction capacitance is then given by,

$$C_{j0} = S\sqrt{\frac{q\epsilon_s N_{\text{epi}}}{2\psi_{bi}}} \tag{2.7}$$

For Schottky diodes with sub-micron contact area, the first-order fringing effect is added as shown below [47],

$$C_j \simeq \frac{\epsilon_s S}{W_d(V_j)} + \frac{3\epsilon_s S}{D_{\text{anode}}} \tag{2.8}$$

$$C_j \simeq \frac{\epsilon_s S}{W_d}\left(1 + b\left(\frac{W_d}{R_{\text{anode}}}\right)\right) \tag{2.9}$$

where R_{anode} and D_{anode} are the radius and diameter of the Schottky contact, respectively, and b is the numerical constant 1.5. Detailed analysis of junction capacitance of Schottky diodes with realistic geometries that are implemented in a 2-D ensemble Monte Carlo simulator can be found in [48].

2.1.4 Series resistance

The diode series resistance is estimated by taking into account: undepleted epi-layer, spreading, and ohmic contact resistance as shown in Fig. 2.4.

- Undepleted epi-layer - Epi-layer resistance can be approximated as

$$R_{\text{epi}} = \frac{t_{\text{epi}} - W_d}{S\ \sigma_{\text{epi}}} \tag{2.10}$$

  where, t_{epi} is the total thickness of the epi-layer and σ_{epi} is the electrical conductivity of epi-layer which is given by,

$$\sigma_{\text{epi}} = qN_{\text{epi}}\mu_{\text{epi}}(N_{\text{epi}}, T) \tag{2.11}$$

μ_{epi} is the low-field electron mobility [42]. Due to the voltage dependence of W_d, R_{epi} varies with voltage as well. However, for analysis purpose, this dependence is neglected and the R_{epi} is calculated when $W_d = 0$.

- Buffer layer - For a point contact diode, the dc series resistance in the buffer region can be approximated as [49],

$$R_{\text{spreading}} = \frac{1}{4\sigma_{\text{buffer}} R_{\text{anode}}} \tag{2.12}$$

where, σ_{buffer} is the electrically conductivity of the buffer region,

$$\sigma_{\text{buffer}} = qN_{\text{buffer}}\mu_{\text{buffer}}(N_{\text{buffer}}, T) \tag{2.13}$$

and N_{buffer}, μ_{buffer} are the doping concentration and corresponding low-

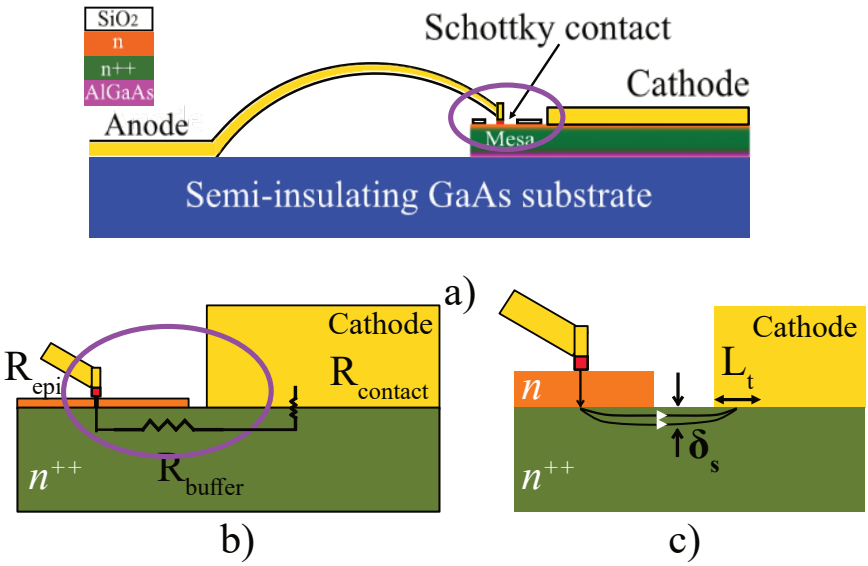

Figure 2.4: Diode series resistance. a) Illustration of the air-bridge and Schottky contact b) Resistance contribution from the epi, buffer layer, and ohmic contact c) Current flow in the highly conductive buffer layer limited by the skin depth δ_s and transfer length L_t.

field electron mobility in the buffer region.

At high frequencies, spreading current in the buffer region is confined to the surface of the buffer region due to the skin effect [50], [51],

$$\delta_s = \sqrt{\frac{2\omega\mu_{\text{buffer}}}{\sigma_{\text{buffer}}}} \tag{2.14}$$

For Schottky diodes with planar geometry, analytical estimation of spreading resistance in the buffer region is not straightforward due to the lateral current flow, and the ohmic contact does not surround the Schottky contact by 360° [52]. A careful estimation of spreading resistance in a planar diode requires 3D-EM simulation using a FEM solver [51]. Alijabbari *et. al,* reported quasi-vertical Schottky diodes with low parasitics in a monolithically integrated structure [53].

- Ohmic contact - For a vertical diode, the ohmic contact resistance can be estimated using [54], [55],

$$R_{contact} = \frac{\rho_c}{A^*_{ohmic}} \tag{2.15}$$

- Low-field mobility model - electron mobility of electrons at room temperature for the specific doping concentration is calculated using the empirical low-field mobility model by Sotoodeh [42] as shown in Fig. 2.5. With increasing doping concentration, scattering due to impurities increases which in turn reduces the electron mobility.

$$\mu(N,T) = \mu_{min} + \frac{\mu_{max}(\frac{T_0}{T})^{\theta_1} - \mu_{min}}{1 + \left(\frac{N}{N_{ref}(\frac{T}{T_0})^{\theta_2}}\right)^{\lambda}} \tag{2.16}$$

where, T_0 is room temperature, μ_{min} and μ_{max} is 500 and 9000 $\text{cm}^2/\text{V.s}$, respectively and N_{ref} is 6×10^{16} cm^{-3}. θ_1, θ_2 and λ are fitting constants for majority carriers: 0.39, 2.1, and 3.0 [42].

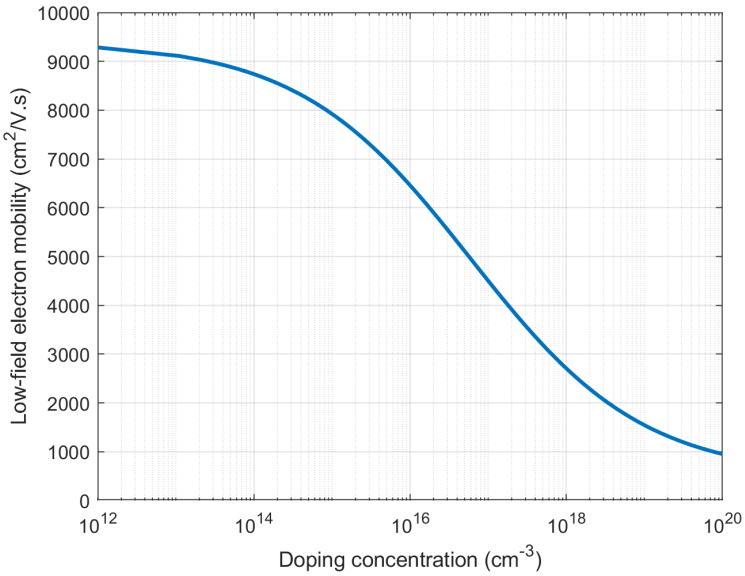

Figure 2.5: GaAs Electron mobility vs. doping concentration calculated using the empirical low-field mobility model [42].

2.1.5 Cut-off frequency

Cut-off frequency is an important figure of merit to compare the performance of Schottky diode based mixers and multipliers in THz applications. It is calculated using the formula given below,

$$f_c = \frac{1}{2\pi R_s C_{j0}} \tag{2.17}$$

It is critical to reduce the series resistance and junction capacitance for increasing the cut-off frequency. Reducing the Schottky contact area will reduce the C_{j0} but increase R_s. On the other hand, increasing the epi-layer doping concentration N_{epi} will reduce R_s but increase C_{j0}. In addition, high N_{epi} will narrow the depletion width W_d thereby increasing the tunneling current which will in turn increase the ideality factor η. As a result, it will worsen the diode's non-linearity. Hence, it is a trade-off between the cut-off frequency

and the mixer performance [56].

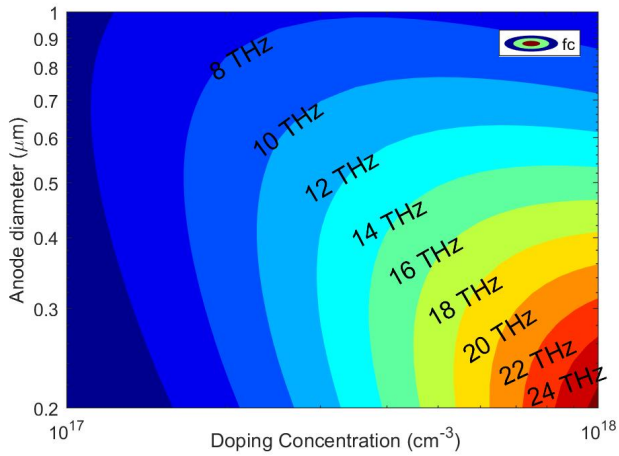

Figure 2.6: Cut-off frequency as a function of Schottky contact area and doping concentration.

2.2 Mixers

Mixers are also referred to as frequency converters utilising the non-linear *I-V* characteristic of a device (diode or transistor) to convert a high-frequency signal to low-frequency or vice-versa. The process is called frequency down-conversion or up-conversion, respectively. Heterodyne receivers utilise two signals: an RF signal that carries the information and an LO signal generated by a local oscillator source. In a THz receiver system, the IF signal is typically amplified using a low-noise amplifier (LNA) [57] and later analysed in the receiver back-end. Fig. 2.7 shows the illustration of a THz heterodyne receiver. The commonly used mixer symbol and the frequency conversion is shown in Fig. 2.8. When the frequency conversion or mixing process is achieved using non-linear resistance, the device is referred to as a resistive mixer [58], [59]. When accomplished using non-linear reactance, it is called parametric mixers [60]. Different mixer topologies utilising diodes as a mixing element are summarised below.

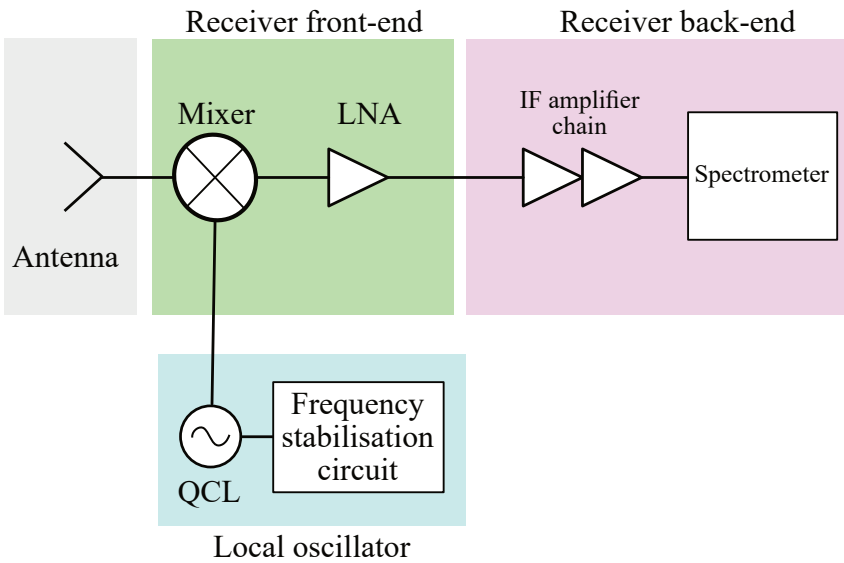

Figure 2.7: Illustration of the THz heterodyne receiver showing the front, back-end receiver and the local oscillator chain.

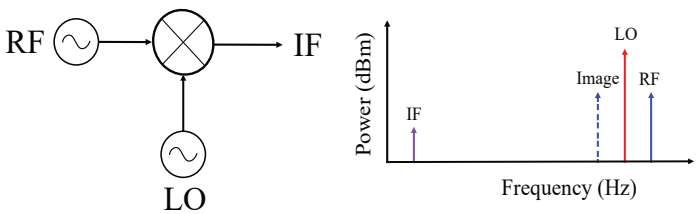

Figure 2.8: Mixer symbol - A three port device with two inputs and one output port for the IF signal.

2.2.1 Single-ended diode mixer

A single-ended mixer topology consists of a single mixing element (diode) and filters for transmission and suppression of the signals, as shown in Fig. 2.9. The mixing process occurs due to the diode's non-linear current-voltage characteristic (I-V), explained as follows.

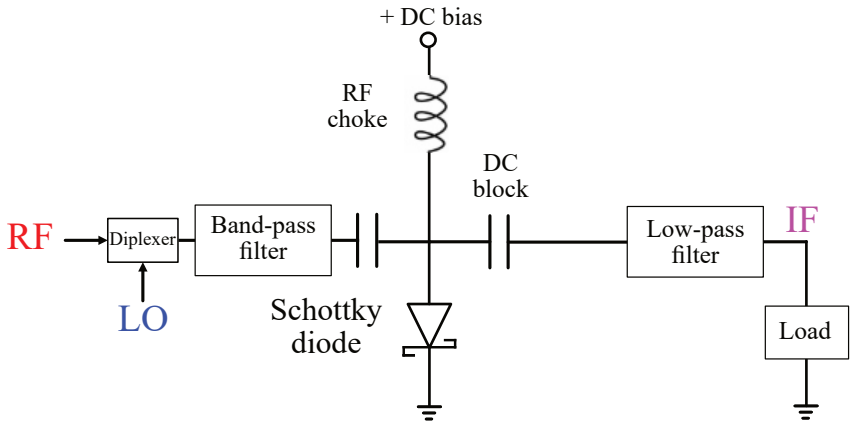

Figure 2.9: Schematic of a single-ended diode mixer.

The incoming signals (RF and LO) can be expressed as,

$$V_{\mathrm{RF}}(t) = V_{\mathrm{RF}} cos(\omega_{\mathrm{rf}} t) \tag{2.18}$$

$$V_{\mathrm{LO}}(t) = V_{\mathrm{LO}} cos(\omega_{\mathrm{lo}} t) \tag{2.19}$$

where, $\omega_{\mathrm{rf}} = 2\pi f_{\mathrm{rf}}$ and $\omega_{\mathrm{lo}} = 2\pi f_{\mathrm{lo}}$. The frequency mixing process is due to the non-linear current-voltage characteristic of the mixing element such as a diode or transistor. Using Taylor series, the diode current can be expressed as,

$$i(t) = a_0 + a_1 v(t) + a_2 v^2(t) + a_3 v^3(t) + ... \tag{2.20}$$

$$v(t) = V_{\mathrm{RF}}(t) + V_{\mathrm{LO}}(t) \tag{2.21}$$

and is expanded as,

$$\begin{aligned} i(t) = a_0 &+ a_1[V_{\mathrm{RF}}(t) + V_{\mathrm{LO}}(t)] \\ &+ a_2[V_{\mathrm{RF}}(t) + V_{\mathrm{LO}}(t)]^2 \\ &+ a_3[V_{\mathrm{RF}}(t) + V_{\mathrm{LO}}(t)]^3 \end{aligned} \tag{2.22}$$

$$i(t) = a_2[V_{\mathrm{RF}}(t)^2 + V_{\mathrm{RF}}(t)^2 + 2V_{\mathrm{LO}}(t)V_{\mathrm{RF}}(t)] \tag{2.23}$$

$$i(t) = a_2 V_{\mathrm{RF}} V_{\mathrm{LO}}[cos(\omega_{\mathrm{rf}} + \omega_{\mathrm{lo}})t + cos(\omega_{\mathrm{if}})t] \tag{2.24}$$

Equation 2.24 consists of a sum and difference of the input signal frequencies. The sum frequency term $\omega_{\mathrm{rf}} + \omega_{\mathrm{lo}}$ is approximately twice the RF signal whilst the difference frequency $\omega_{\mathrm{rf}} - \omega_{\mathrm{lo}}$ is the desired IF signal. A low-pass filter will remove the sum frequency term and all the undesirable higher order mixing products. In this thesis, the single-ended diode mixer utilises the n^{th} harmonic of the LO signal to generate the IF signal [61] and hence is referred to as harmonic mixer.

$$f_{\mathrm{IF}} = f_{\mathrm{RF}} - nf_{\mathrm{LO}} \tag{2.25}$$

where, n is the harmonic index.

2.2.2 Sub-harmonic mixer

The sub-harmonic pumped mixers at millimetre-wave applications are realised using anti-parallel diode topology [62]. It was first proposed by Cohn *et. al* in 1975 [63]. The schematic of the anti-parallel diode mixer is as shown in Fig. 2.10.

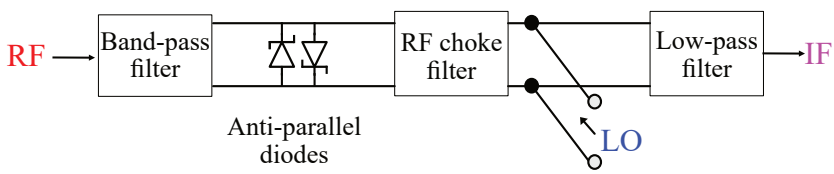

Figure 2.10: Schematic of the sub-harmonic mixer

It utilises a LO signal which is half of the RF signal ($f_{LO} = \frac{1}{2} f_{RF}$), which is advantageous in THz applications where the LO signal generation is made possible using frequency multipliers based on solid-state devices [64]. Diodes are often connected in series or parallel to reject certain mixing products or harmonics. The desired output frequency is generated by mixing the RF signal with the second harmonic of the LO signal.

$$\omega_{\mathrm{IF}} = \omega_{\mathrm{RF}} - 2\ \omega_{\mathrm{LO}} \tag{2.26}$$

The I-V characteristic of an anti-parallel diode mixer is,

$$\begin{aligned} I &= I_1 + I_2 \\ &= f(V) - f(-V) \\ &= [aV + bV^2 + CV^3 + ...] - [-aV + bV^2 - cV^3 + ...] \\ &= 2aV + 2CV^3 + ... \end{aligned} \tag{2.27}$$

The frequency mixing process results in only odd-order components and no even-order components. When employed as a sub-harmonic mixer, it utilises the second-harmonic or third-order mixing product to generate the IF and suppresses the fundamental mixing product. On the other hand, an anti-series mixer generates only even-order components [46].

2.2.3 Idler terminations

Saleh [58] has proposed different schemes and mixer topologies based on reactive idler terminations. The undesired out-of-band frequencies are referred to as idlers. The mixer's performance can be improved depending on the idler terminations (short or open circuit).

All idlers are grouped into one and terminated by an open or short circuit in the unitary division scheme. These mixers are called Z-, and Y-mixers, respectively. In the binary division scheme, the out-of-band frequencies are divided into odd and even frequencies. Grouping even and odd idler frequencies and terminating them with a short and open circuit are referred to as H-mixer, and vice-versa is a G-mixer Table. 2.2.

Table 2.2: Mixer classification system based on idler terminations

Idlers ω_{2n}	Idlers ω_{2n+1}	Assigned name
Short	Short	Y-mixer
Open	Open	Z-mixer
Open	Short	G-mixer
Short	Open	H-mixer

2.3 Mixer conversion loss

Conversion loss is a useful figure of merit when evaluating the performance of the mixers. The mixer conversion is given by,

$$L = P_{\mathrm{RF,in}}/P_{\mathrm{IF,out}} \tag{2.28}$$

where, $P_{\mathrm{RF,in}}$ and $P_{\mathrm{IF,out}}$ are input RF frequency and output intermediate frequency respectively. When no energy is dissipated in the out-of-band frequencies (idlers), the theoretical limit of the conversion loss is 3 dB for a double side-band mixer (DSB) [65]. In reality, the mixer conversion loss is degraded due to various factors such as: diode series resistance, power dissipation in idlers, impedance matching, and self heating effects [66].

2.4 Mixer noise

Noise is an important figure of merit for mixers. The major contributors of noise in Schottky diodes are

- Thermal noise, also called Johnson or Nyquist noise, originating from discrete nature of electric charges [67]-[68].
- Shot noise is generated due to current flow across the junction [69].

The shot noise current can be modelled as a current source parallel to I_j and thermal noise associated with the resistance contributions from epi-layer R_{epi} and buffer region R_{buffer} can be modelled as a series voltage source [70] as shown in Fig. 2.11.

$$i_{\mathrm{shot}} = 2qI_jB \tag{2.29}$$

where, I_j is the instantaneous current flow across the junction and the equivalent noise temperature of the junction is given by,

$$T_{\text{shot}} = \frac{qV_j}{2k_B} \tag{2.30}$$

The mean square voltage amplitude of thermal noise is given by,

$$v_{\text{thermal}} = 4kTBR \tag{2.31}$$

where, B is the bandwidth in Hz and R is the resistance.

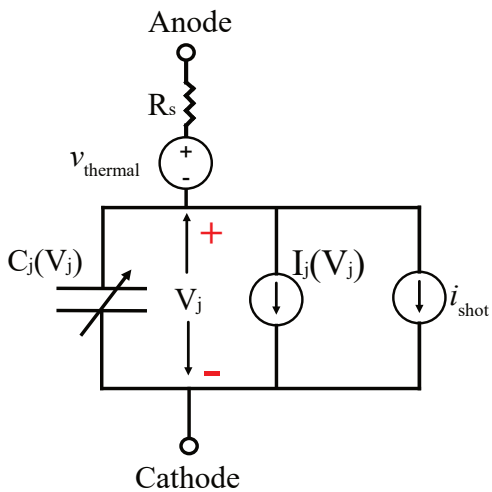

Figure 2.11: Equivalent circuit of noise sources in Schottky diode

CHAPTER 3

Design and fabrication of harmonic mixer

This chapter describes the mixer topology, diode selection and modelling, single-ended Schottky diode mixer design, integrated mixer circuit fabrication, mixer blocks machining, and mixer assembly.

3.1 Design approach

Mixer block - Waveguide based mixers and multipliers are often realised in an E-plane split block configuration as it does not affect the current distribution of the fundamental waveguide (TE_{10}) mode. It eases the milling process of rectangular waveguides (1:1 aspect ratio) [71]–[73]. In addition, metal-waveguide mixers are attractive due to their direct thermal and grounding connections [74].
RF feedhorn - At THz frequencies, loss due to the atmospheric attenuation is high. Hence, the RF feedhorn was directly integrated into the mixer block. The diagonal feedhorn is an ideal candidate since they do not require additional waveguide transitions [75].
LO chain - The LO signal is generated from a 600-GHz, $\times$64-active multiplier

chain, which has a WM-380[1] output waveguide with UG-387 flange interface [76].

Diode modelling - For a given Schottky contact area, diode series resistance (R_s) and zero-bias junction capacitance (C_{j0}) was estimated using the analytical model presented in chapter 2.

The embedding impedances that offers low conversion loss for an ideal Z-mixer was estimated at RF, LO, IF using an in-built diode model in the circuit simulator (ADS) [paper A]. Next, 3D-electromagnetic (EM) modelling is carried out in the FEM solver (HFSS). The embedding impedances at RF and LO frequencies were presented to the diode, and the mixer performance is evaluated in terms of conversion loss and RF/LO return loss. Finally, sensitivity analysis of critical parameters was carried out to check the robustness of the design [Paper B].

3.1.1 Mixer topology

The single-ended diode mixer topology, as shown in Fig. 3.1 is chosen due to its simplicity and to ease the circuit fabrication process.

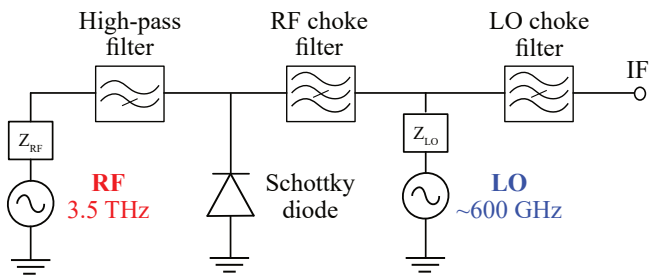

Figure 3.1: Schematic of the single-ended diode harmonic mixer. Z_{RF} and Z_{LO} are the optimum embedding impedance at the RF and LO frequencies respectively. Upon mixing, 6^{th} harmonic of the LO signal generated from the multiplier chain will result in a down-converted IF signal at 200 MHz.

[1]RF waveguide name designation. 'W' stands for waveguide, 'M' for metric, and the number is the waveguide width in μm

3.1.2 Diode selection

The traditional "vertical" whisker contact Schottky diodes offer low parasitic capacitance but are susceptible to vibrations and not reliable as the Schottky contact diameter decreases [77]. In 1987 Bishop *et al.* proposed a "planar" Schottky diode technology, paving the way for the development of robust, reliable, and mechanically stable Schottky-diode structures [78].

The Schottky contact area is preferably less than 0.2 μm^2 and epi-layer with 6×10^{17} cm^{-3} doping concentration was chosen to reduce the parasitics and to operate below the cut-off frequency. It is followed by a highly doped buffer layer with a concentration of about 5×10^{18} cm^{-3} to facilitate conduction to the ohmic contacts. The thickness of the epi-layer is equal to the depletion width W_d at zero bias, and the buffer layer is 0.5 μm [51]. The top and bottom etch stop layers have different thicknesses due to the tolerances in the front and backside etching process steps.

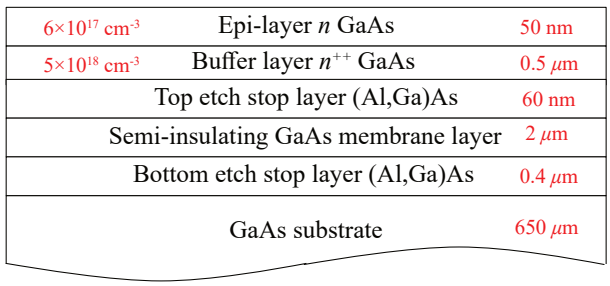

Figure 3.2: Epitaxial material layer structure of a typical THz Schottky diode mixer

Three different Schottky contacts were fabricated (0.14 μm^2 $\pm$ 20%) to tackle problems that may arise due to fabrication tolerances. Fabrication of circuits at high frequencies is often limited due to higher order propagating modes in the supporting GaAs substrate. In order to reduce the circuit losses and parasitics, the integrated diode technology will be realised using suspended stripline technology in 2-μm thick GaAs membrane [79], [80] as shown in Fig. 3.2.

3.1.3 Embedding impedances

Harmonic balance is a commonly used technique to evaluate the mixer performance. It partitions a circuit consisting of both linear and non-linear elements into subcircuits, as shown in Fig. 3.3. The linear circuits are analysed using a multi-port matrix (S- or Y-) in the frequency domain, and the non-linear circuits are modelled using their I-V characteristics are analysed in the time domain. The goal of a harmonic balance simulation is to find a set of voltage waveforms that give the same current in the linear and non-linear subcircuits [46].

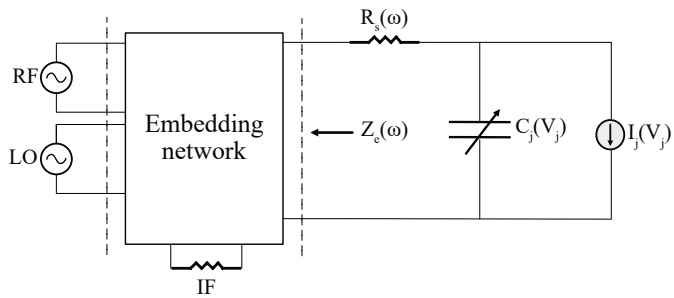

Figure 3.3: Mixer embedding network. The series resistance of the diode and the embedding impedance are analysed in frequency domain. The non-linear junction capacitance and conductance are represented in time domain.

The optimum embedding impedance of a ×6-harmonic mixer was evaluated at RF and LO frequencies using this technique and discussed in detail in [paper A]. The out-of-band frequencies or idlers were assumed to be short-circuited (Z-mixer topology). The optimum impedance at IF is typically very high, around kΩ [81]. The embedding impedance varies as a function of frequency and pump power. In Fig. 3.4 and Fig. 3.5, the optimum embedding impedance at RF and LO frequencies for an LO power of 2 dBm is presented. The simulated conversion loss of 20 dB was obtained for an ideal Z-mixer. Depending on the type of idler terminations, the mixer conversion loss can vary. In reality, it is impossible to present short-circuit terminations to all idlers. Hence, the conversion loss is typically higher, and it increases with increasing harmonic index.

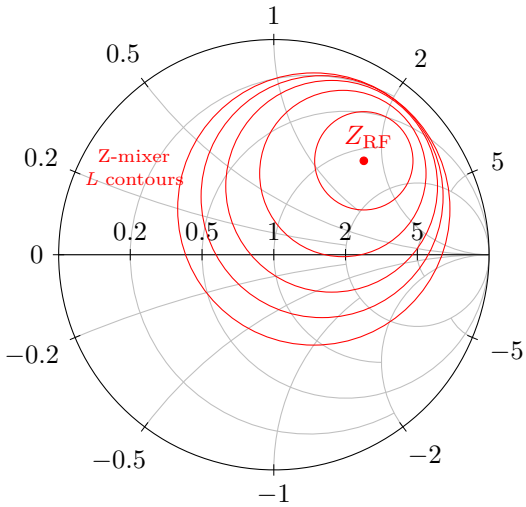

Figure 3.4: Smith chart showing the conversion loss L contours and the RF optimum embedding impedance at 3.5 THz. Contour level: 1 dB.

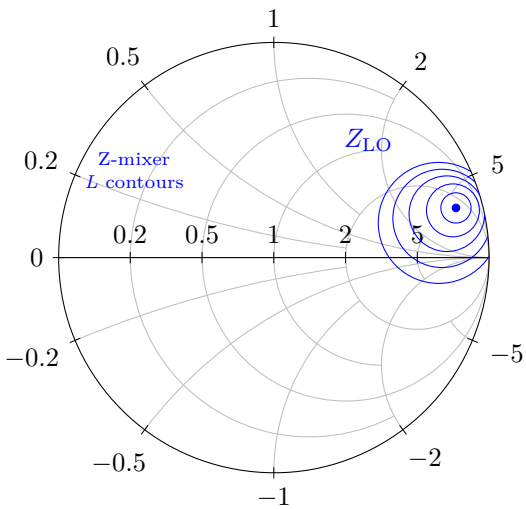

Figure 3.5: Smith chart showing the conversion loss L contours and the LO optimum embedding impedance at 600 GHz. Contour level: 1 dB.

3.1.4 Choke filters

To maximise the coupling of incoming signals to the diode and improve the mixer performance, it is vital to have broad-band filters that can prevent signal leakage and provide isolation between RF, LO and IF chains.

3.1.4.1 Stepped impedance filter

Stepped impedance filters consist of alternating high-low impedance line sections. These sections are realised using suspended stripline technology by varying the width of the strip lines as shown in Fig. 3.6. The 5^{th} order stepped impedance provided isolation of about -18 dB isolation at the centre frequency (3.5 THz).

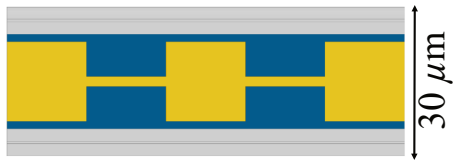

Figure 3.6: 3D-EM model of the planar stepped impedance filter which provides RF signal isolation.

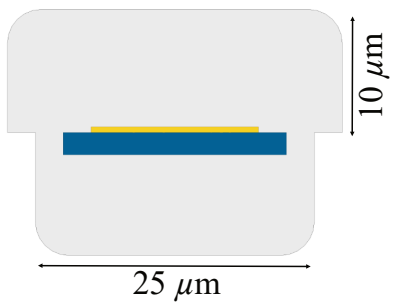

Figure 3.7: Cross section of the RF channel 3D-EM model showing the 2-μm-thick GaAs membrane and 0.5-μm-thick gold striplines defining the stepped-impedance filter.

Fig. 3.7 shows the cross-section of the RF channel showing the stepped impedance

filter defined on a 2-μm GaAs membrane. The top and bottom channels have different widths to account for the misalignment of top and bottom split blocks. The rounded corners arising from the milling process is taken into consideration in the 3D-EM model design. To ensure only the fundamental quasi-TEM mode exists in the RF channel, the height and the width of both top and the bottom channels were optimised. Fig. 3.8 shows there is a single-mode operation up to 3.75 THz.

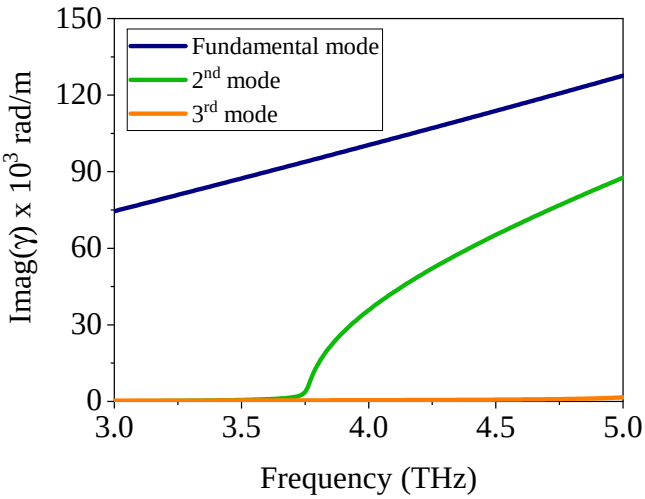

Figure 3.8: Propagation factor versus frequency for fundamental, 2^{nd}, and 3^{rd} order modes in the RF channel.

3.1.4.2 Hammerhead filter

Higher order stepped-impedance filters can provide better signal suppression, but at the expense of having an electrically long circuit. Hence, it is critical to have an electrically short filter that can provide good isolation over a wide bandwidth. Hammerhead filter is a good candidate that satisfies these requirements [Paper B, C]. Fig. 3.9 shows the top view of the LO choke filter suspended using beam leads in the LO channel.

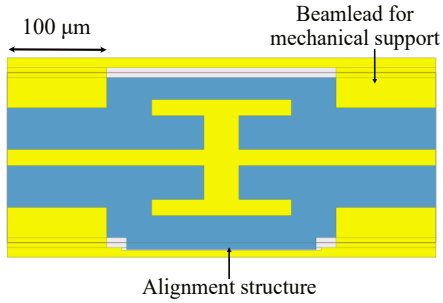

centering

Figure 3.9: 3D-EM model of the LO choke filter realised using a Hammerhead filter. The gold beam leads provides grounding, heat transfer and mechanical support. The asymmetrical GaAs membrane aids in the precise alignment of the circuit in the block.

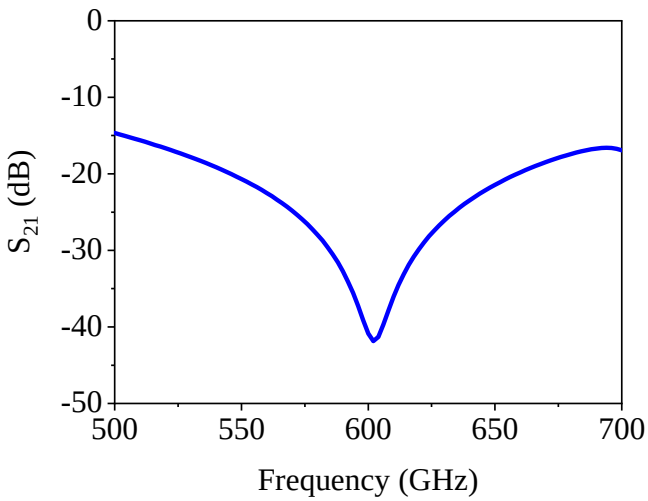

Figure 3.10: 3D-EM simulation response of the hammerhead filter from 500 to 700 GHz with suppression better than -20 dB between 550 to 650 GHz.

Beam leads provide efficient support, heat transfer, electrical grounding, and precise circuit alignment in the E-plane mixer split block. Fig. 3.10 shows the filter response of the designed hammerhead filter with suppression better than

-20 dB between 550 to 650 GHz and high suppression of about -40 dB at the centre frequency.

3.1.5 Harmonic mixer

Fig. 3.11 shows the full 3D-EM model of the 3.5-THz, ×6-harmonic mixer, including the RF/LO waveguides and channels and the integrated mixer circuit including the planar Schottky diode and choke filters. The RF port (WM-64), LO port (WM-380), and the IF port were assigned with a waveguide port. The harmonic mixer was evaluated using the multi-frequency adaptive mesh at RF and LO frequencies, resulting in about >200 000 tetrahedrons. [Paper C] presents the upgraded design and preliminary simulation results of a harmonic mixer operating at 4.7 THz.

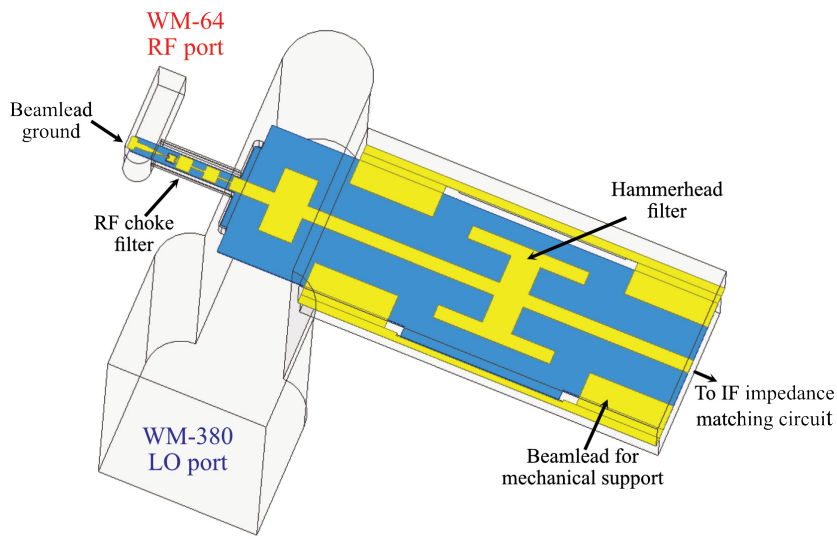

Figure 3.11: Full 3D-EM model of the 3.5-THz, ×6-harmonic Schottky diode mixer.

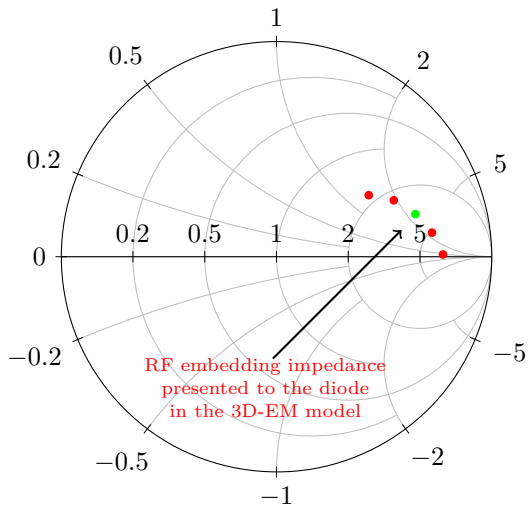

Figure 3.12: Smith chart showing the RF embedding impedance presented to the diode in the 3D-EM model from 3.4 to 3.6 THz shown in red dots and the green dot represent the center frequency

3.1.6 Horn antenna

It is advantageous for terahertz heterodyne receivers to have feedhorns that can maximise signal coupling to detectors and have low cross polarisation. Corrugated horn is an attractive candidate due to their high sensitivity, and low cross polarisation [82]. However, at THz frequencies, it is difficult to realise them due to fabrication tolerances. Other feedhorn profiles such as Pickett-Potter horns [83], [84] and multi-flare angle horns are widely used as well, but they require a circular to rectangular waveguide transition. On the other hand, diagonal horns can be directly integrated with the rectangular waveguides [85]. Nevertheless, they have poor efficiency due to their high cross polarization component.

In this thesis, the RF feedhorn is based on a standard diagonal horn design described by Johansson and Whyborn [86]. A diagonal horn with an aperture size of 384×384 μm^2, corresponding to a flare angle of 5.4°, resulted in a simulated directivity of about 23 dBi.

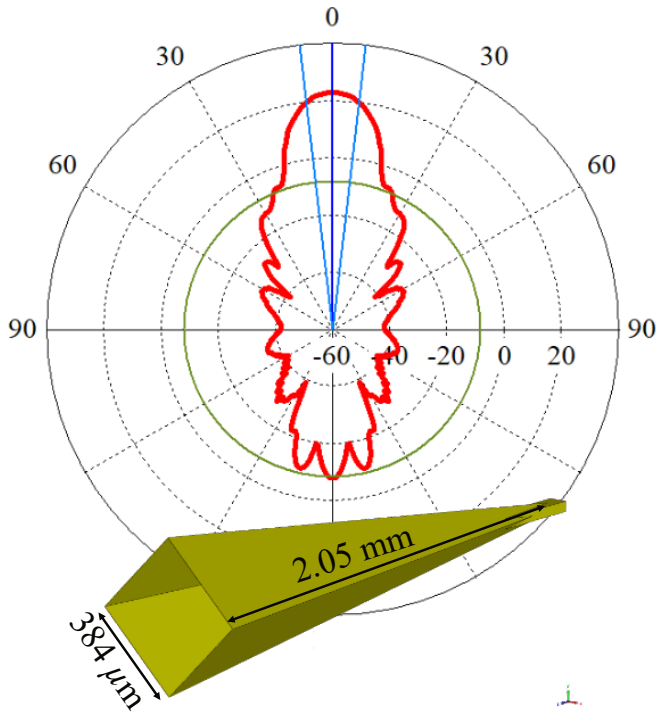

Figure 3.13: 3.5-THz diagonal horn. (Top) Simulated H-plane radiation pattern of the diagonal horn. (Bottom) 3D-EM model of the feedhorn.

3.1.7 IF impedance transformer

An impedance transformer is required to transform the mixer IF impedance 150 Ω to 50-Ω IF output. It can be realised using a quarter-wavelength transformer, resulting in a very narrow bandwidth. To increase the bandwidth, multi-section impedance transformers such as Chebyshev, and binomial are commonly used[87]. A three-section Chebyshev impedance transformer, as shown in Fig. 3.14. The simulated insertion loss was less than 0.3 dB in the frequency range from 1.5 to 7 GHz. To realise a compact front-end receiver module, it is beneficial to integrate the LNA to the mixer module as presented in [88]. This approach can minimise the ripples caused due to the mismatch between the mixer and LNA.

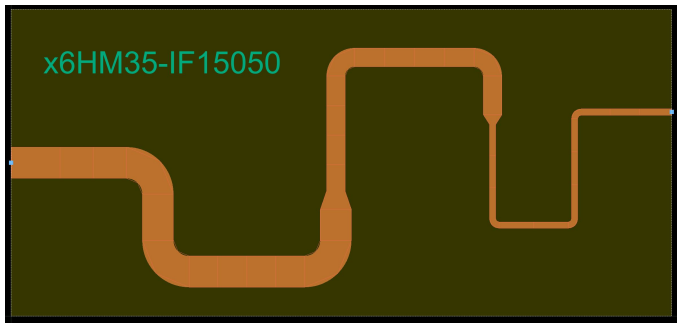

Figure 3.14: Picture showing the layout of the three-section Chebyshev 150 to 50 Ω impedance transformer.

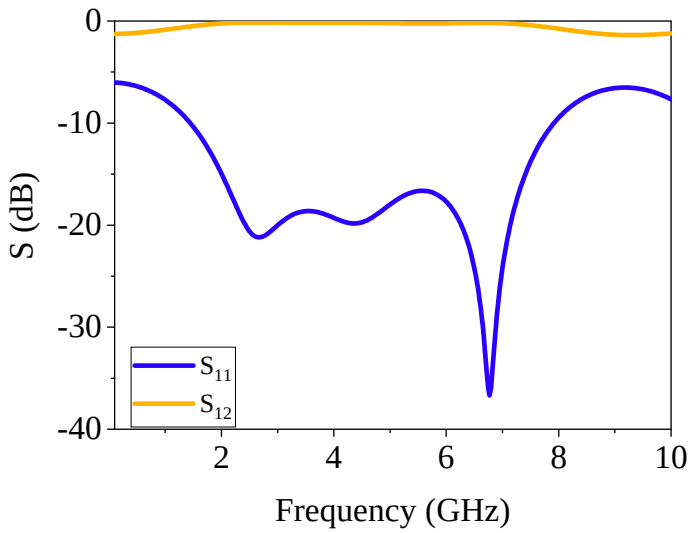

Figure 3.15: Return loss and insertion loss of the three-section Chebyshev impedance transformer. Losses in the gold traces are taken into account in the 3D planar EM simulator based on Method of Moments (MoM) in the circuit simulator.

3.1.8 Sensitivity analysis

Sensitivity analysis was performed to check the robustness of the harmonic mixer. The parameters with critical tolerances are varied by 10% of their original value to approximate the partial derivatives [89] as shown in Table.3.1. The relative sensitivity coefficient is given by,

$$S_x^L = \frac{\Delta L/L_0}{\Delta x/x_0} \tag{3.1}$$

where $\Delta L = L_x - L_0$ denotes the change in the conversion loss, L_0 the nominal conversion loss, Δx the relative variation of the parameter in the study, and x_0 the nominal value of the parameter. The relative sensitivity coefficient was then calculated by studying the mixer conversion loss and is plotted as shown in Fig. 3.16. The diode ideality factor (η) has the strongest influence on the conversion loss of the mixer due to its influence on the diode non-linearity.

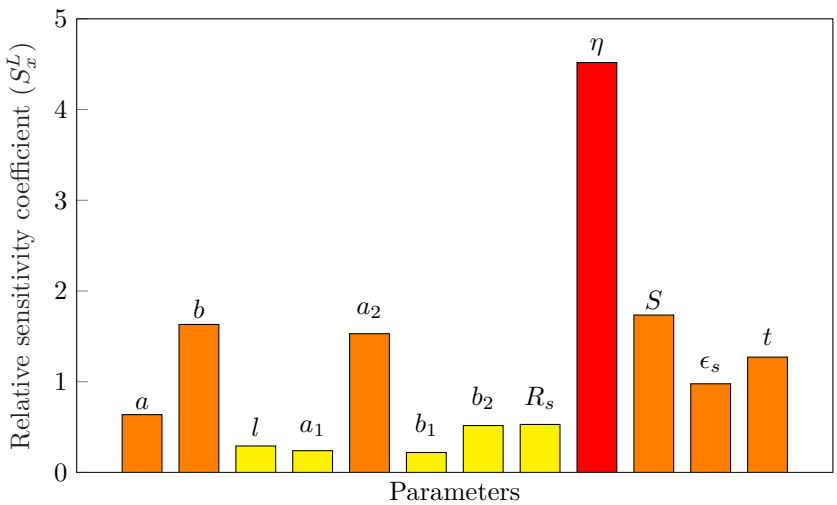

Figure 3.16: Robustness of the 3.5-THz, ×6-harmonic Schottky diode mixer. A sensitivity analysis showing the influence of the circuit design and diode model parameters listed in Table 3.1. The following parameters were assigned to the harmonic-balance simulation: RF = 3.5 THz, IF = 5 GHz, LO power = 2 dBm, RF power = −50 dBm, and no dc bias.

Table 3.1: List of the circuit parameters studied in the sensitivity analysis

Block	RF waveguide width	$a = 2b$	64 μm
	RF waveguide height	b	32 μm
	RF backshort	l	30 μm
	RF filter channel width (top)	a_1	30 μm
	RF filter channel width (bottom)	a_2	25 μm
	RF filter channel height (top)	b_1	10 μm
	RF filter channel height (bottom)	b_2	10 μm
Diode	Series resistance	R_s	25 Ω
	Ideality factor	η	1.2
	Schottky junction area	S	0.11 μm^2
GaAs Membrane	Relative permittivity	ϵ_s	12.9
	Membrane thickness	t	2 μm

3.2 Fabrication of harmonic mixer circuits

Fig. 3.17 shows the scanned electron micrograph of the planar, integrated, $\times$6-harmonic mixer circuits on the supporting GaAs wafer. [Paper B] presents the detailed fabrication process.

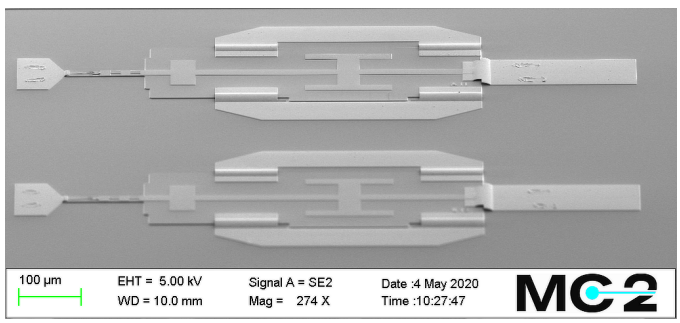

Figure 3.17: SEM picture of the single-ended integrated Schottky diode mixer circuits on the supporting wafer.

3.3 Mixer assembly

Mixer block fabrication - The mixer was machined in an E-plane split aluminium block using a high-speed, micrometre precision CNC milling tool (KERN Evo). For details of the milling tools used in this process, refer to [Paper B].
Assembly - The integrated harmonic mixer circuit was assembled on an E-plane split block. The beamleads aids in heat transfer from the diode to the surrounding metal and provide mechanical support as the integrated circuit is suspended in the block, as shown in Fig. 3.18. The IF beamlead is punched into the quartz circuit using a ceramic wedge. The quartz circuit and the PCB are connected using a small bond wire, and finally, the SMA connector is soldered to the PCB board. Finally, the harmonic mixer block is connected to the 600-GHz LO multiplier chain as shown in Fig. 3.19.

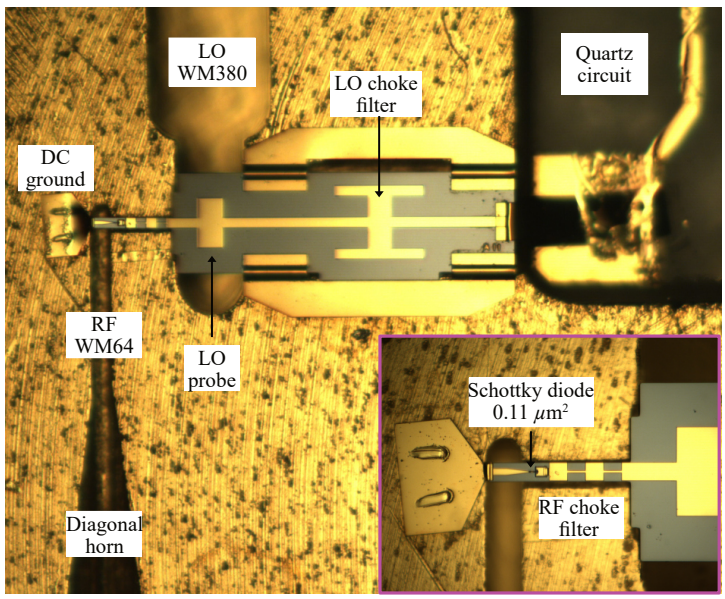

Figure 3.18: Micrograph showing the integrated harmonic mixer circuit assembled on the bottom E-plane split block. Inset: Micrograph showing the RF circuitry and the Schottky diode.

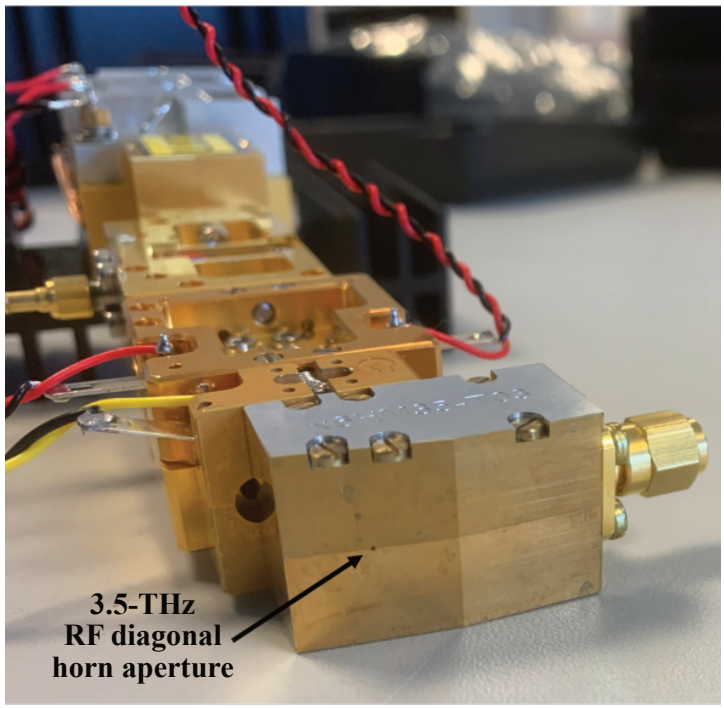

Figure 3.19: Photograph of the harmonic mixer connected with the 600-GHz, LO multiplier chain. The aperture of the 3.5-THz diagonal feedhorn is indicated in the picture.

CHAPTER 4

Characterisation of harmonic mixer

Integrated 3.5-THz, ×6-harmonic mixer circuits with Schottky contact area 0.11 and 0.14 μm^2 were assembled on the mixer blocks. Both showed similar performance in terms of mixer conversion loss [Paper B], [90]. The mixers were successfully employed in a phase-locked loop application for frequency stabilisation of the QCL, which yielded 40 dB and 30 dB SNR at 3.5 THz and 4.7 THz respectively [91]. In this chapter, dc and RF characterisation results of the harmonic mixer with a Schottky contact area of 0.11 μm^2 is presented in detail.

4.1 DC characterisation

Estimation of parameters such as diode series resistance R_s, ideality factor η, and saturation current I_{sat} are crucial to model the Schottky diode's dc non-linear behaviour and to find a safe operating point. For accurate R_s measurements, it is essential to eliminate the losses in cable and connectors, and it is achieved by using four-point or Kelvin probe sensing. It consists of force-and-sense probe pairs which are used for current-carrying and voltage sensing, respectively, as illustrated in Fig. 4.1. A static current-voltage (I-V)

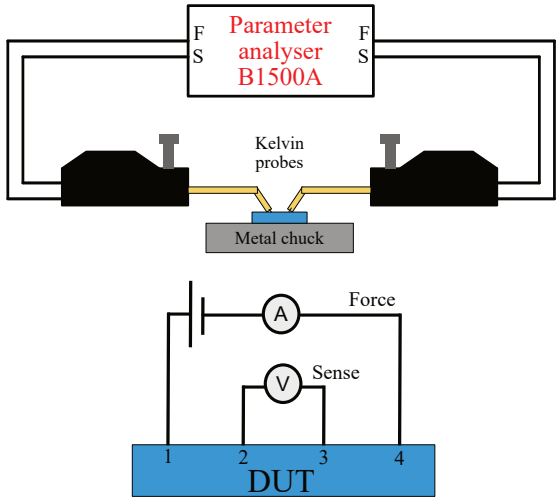

Figure 4.1: Illustration of the dc measurement setup (Top) and the principle of four terminal sensing (Bottom).

measurements by either varying the dc voltage or current.

Self-heating effects in semiconductor devices have a considerable effect on device performances [92]. In particular, extraction of these parameters is greatly influenced by temperature variations in the Schottky junction. To isolate the effects due to self-heating, pulsed *I-V* measurement is a widely used technique. A voltage or current pulse with a width less than the device thermal time constant τ_{th} is applied across the diode. The thermal time constant is $\tau_{th} = R_{th}C_{th}$, where, R_{th} and C_{th} are thermal resistance and capacitance, respectively.

Before releasing the integrated mixer circuits from the wafer, static *I-V* measurements were performed on-wafer using Kelvin probes at room temperature. Fig. 4.2 shows the comparison of the IV measurement and ideal diode model from the circuit simulator for 0.11 μm^2 Schottky contact area. The following parameters were extracted [93] by fitting the IV curves from the ideal diode model with the measurements: $R_{\mathrm{s}} = 50\ \Omega$, $\eta = 1.24$, $I_{\mathrm{sat}} = 9$ fA.

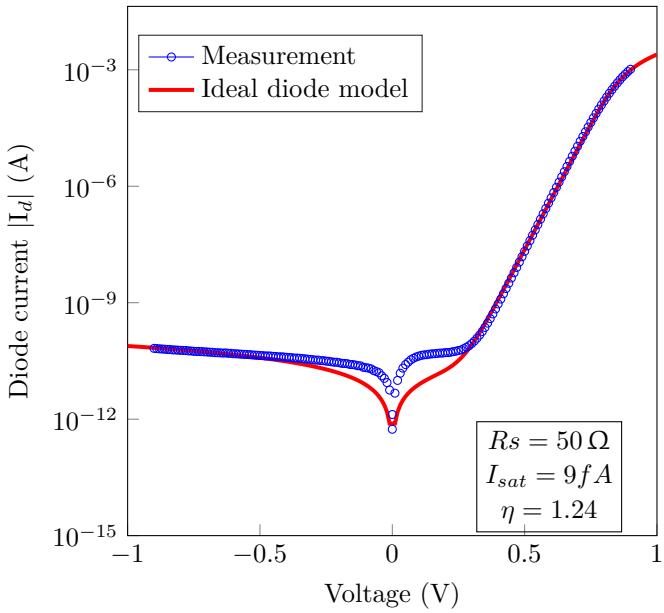

Figure 4.2: Comparison of IV measurement and ideal diode model for a Schottky contact area 0.11 μm^2.

4.2 RF characterisation

Fig. 4.3 and 4.4 shows the photograph and schematic of the RF mixer characterisation set up at the German Aerospace Center (DLR), Berlin. The QCL is placed in a compact Sterling cryocooler which provides thermal stabilisation. The typical operating temperature of the QCL is around 50 K with temperature stability < 1 mK. The signal from the 3.5-THz QCL was focused on the harmonic mixer using a TPX lens. The 3.5-THz, $\times$6-harmonic, single-ended Schottky diode mixer has an integrated diagonal feed horn that receives the incoming THz radiation. The harmonic mixer was pumped using a 600-GHz, $\times$64-active multiplier chain based on three cascaded Schottky $\times$2 MMIC multipliers from Chalmers University of Technology and a commercial $\times$8 active E-band drivers from Millitech (Smiths interconnect). A bias tee was used to apply dc voltage to the harmonic mixer. The IF signal generated from the mixer is amplified using a low noise amplifier (LNA), and the signal is read

out using a spectrum analyser.

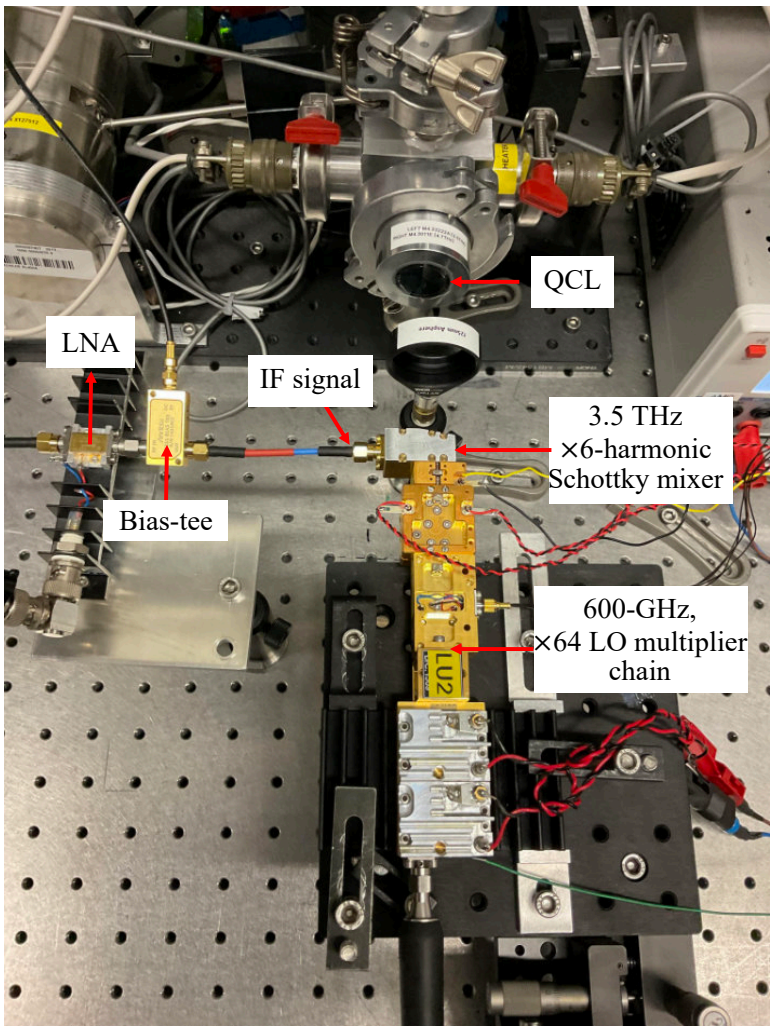

Figure 4.3: A photograph of the measurement setup at the German Aerospace Center (DLR), Berlin. The 3.5-THz QCL is placed in a Sterling cryocooler, the THz beam generated from the QCL is focused to the harmonic mixer using a TPX lens.

4.2.1 3.5-THz, ×6-harmonic mixer

The THz beam from the QCL is focused using a Polymethylpentene (TPX) lens with a desirable beam waist (below 200 μm). The beam profile was evaluated using a microbolometer camera as shown in Fig. 4.5. The side lobes

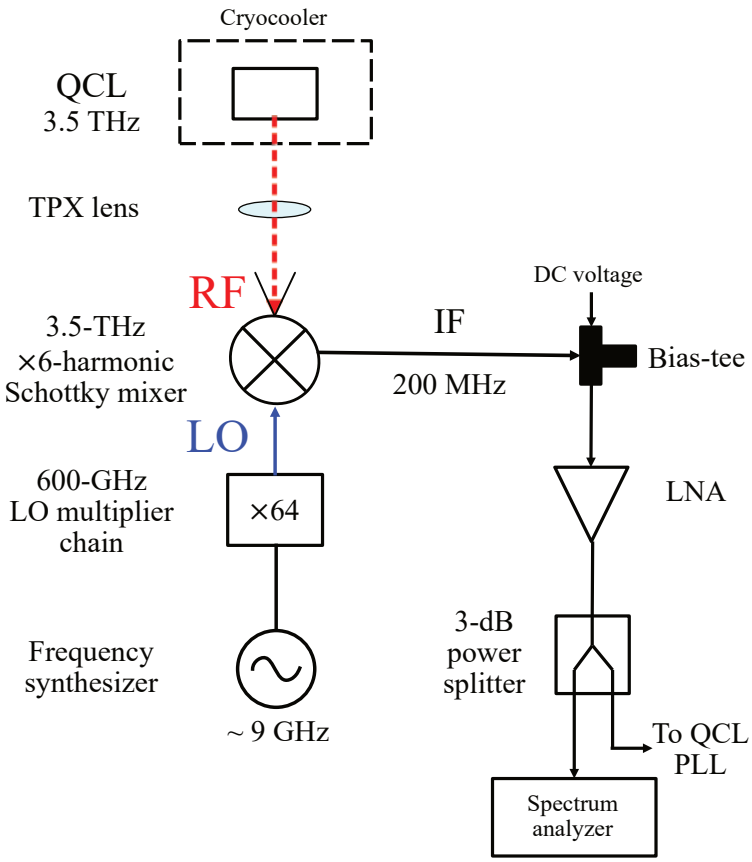

Figure 4.4: A schematic of the RF mixer characterisation setup showing the 3.5 THz-QCL, harmonic mixer and 600 GHz LO multiplier source. The IF signal generated at 200 MHz is amplified using an LNA and read out in the spectrum analyser.

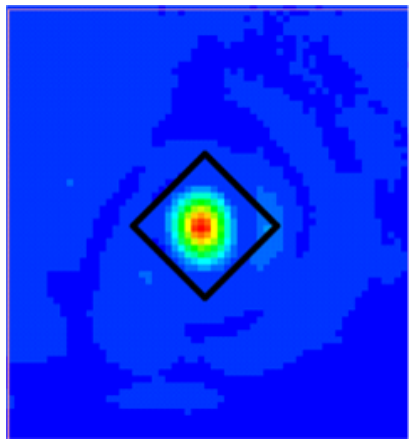

Figure 4.5: Picture of the THz beam profile from 3.5-THz QCL measured using a THz camera. The aperture of the RF diagonal feed horn of the harmonic mixer is indicated as a black line. The measured beam waist was ≈ 170 μm.

are caused due to the diffraction from the TPX lens. The harmonic mixer connected to the 600-GHz multiplier chain was then aligned using an XYZ micrometre stage. The absolute power measurement was carried out using a Thomas Keating power meter at the mixer interface, eliminating the need to de-embed the atmospheric attenuation at 3.5 THz. Absolute power measurements at terahertz frequencies has been quite challenging due to: temperature drift, slow response time, poor sensitivity and frequency dependent calibration.

The THz beam from the QCL was amplitude modulated using a mechanical chopper with a frequency of 15 Hz. A TPX lens was used to focus the beam, and the power meter head was aligned such that the incoming signal was incident at the Brewster angle. The frequency was determined with high precision (< 1 MHz) by measuring the absorption of the QCL radiation guided through an absorption cell filled with methanol and comparing this spectrum with a reference spectrum of methanol.
Conversion loss of the harmonic mixer was determined by taking the difference between the RF and IF power. Losses in the cables, as well as the connectors and LNA's gain, were considered. In Fig. 4.6 the applied dc voltage to the

mixer and LO power from the ×64, 600-GHz, LO multiplier chain is varied, and the corresponding conversion loss is plotted as a 2D contours. At low LO power and bias, the conversion is higher than 100 dB. Increasing the LO power or dc bias improves the mixer performance. Conversion null features which are caused due to destructive interference of competing mixing products are also observed [94]. The current safety limit of the diode (1 mA) sets the higher limit on the LO power and dc bias that can be applied to the mixer.

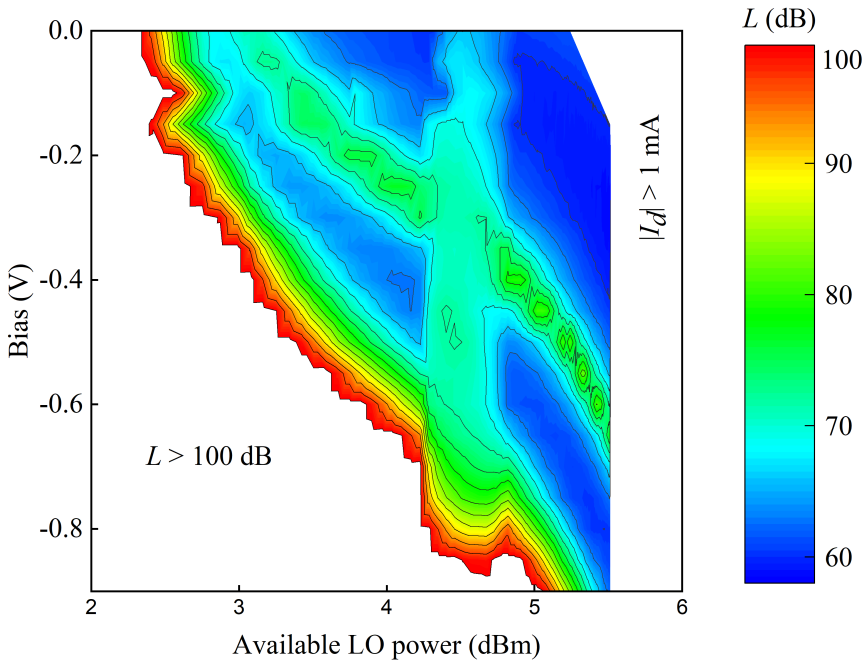

Figure 4.6: Measurement results. Conversion loss contours versus LO power and bias of mixer M1 measured at an IF of 200 MHz, an RF of 3.443 THz, and for an LO signal at 573.3 GHz. The measured RF power at the mixer interface was about −3 dBm and the available LO power was about 5.6 dBm at 573 GHz.

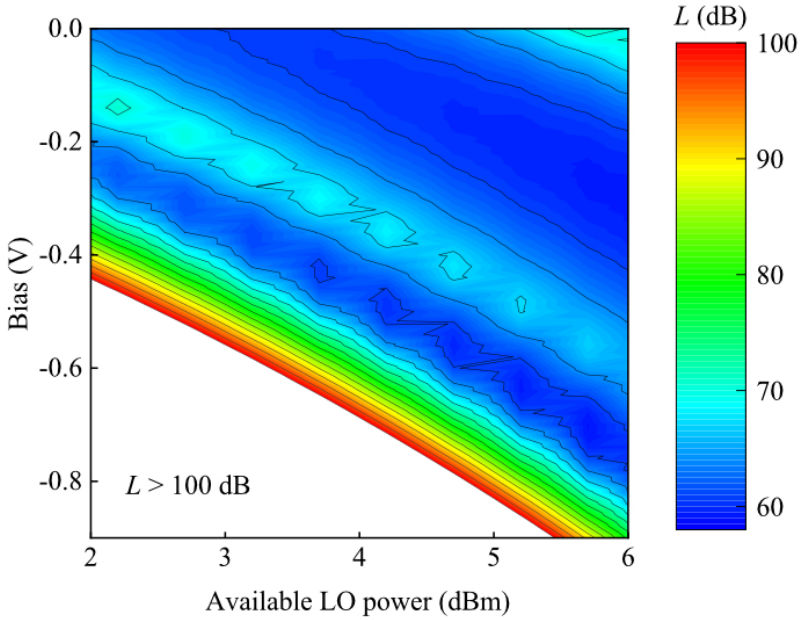

Figure 4.7: Simulation results. Conversion loss contours versus bias and LO power simulated at an IF of 200 MHz, an RF of 3.443 THz, and for an LO signal at 573.3 GHz. The ideal-diode model in the simulation was assigned with parameters extracted from the dc measurements (R_s = 50 Ω, $\eta = 1.24$, $I_{sat} = 9$ fA).

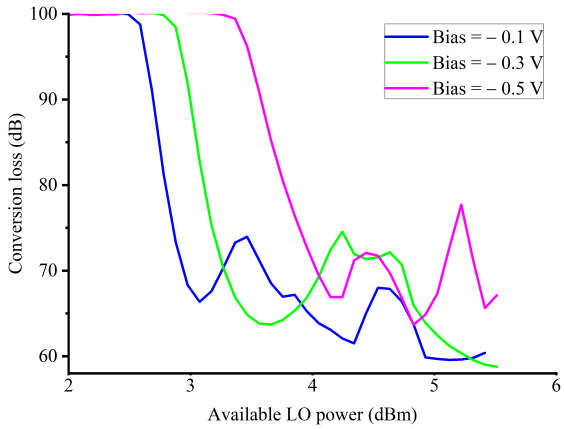

Figure 4.8: Horizontal cross section from Fig. 4.6. Conversion loss versus LO power at constant dc bias.

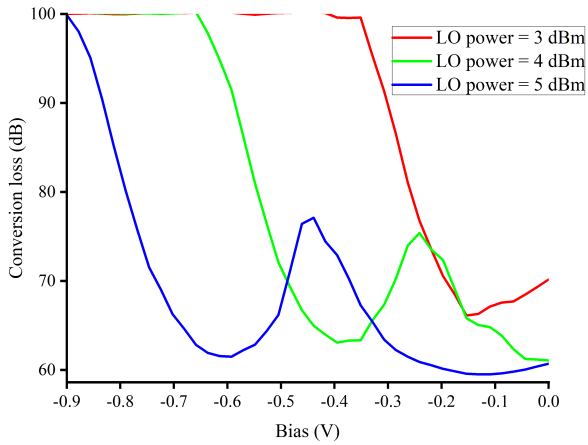

Figure 4.9: Vertical cross section from Fig. 4.6. Conversion loss versus bias at constant LO power. Conversion null features caused due to destructive interference arising from competing mixing products can be observed to move along lower bias points with increasing LO power.

Horizontal cross-sections (i.e constant dc bias) and vertical cross-sections (i.e constant LO power) were taken from Fig. 4.6 and plotted in Fig. 4.8, and Fig. 4.9, respectively. The conversion null features move towards low bias values with increasing LO power as shown in Fig. 4.9. To understand the harmonic mixer's performance in Fig. 4.6, a large-signal harmonic balance simulation was performed. The ideal diode model described in chapter 2 was updated with parameters extracted from the dc measurements, and the simulated conversion loss contours are presented in Fig. 4.7. A vertical cross-section from the measurements Fig. 4.6 and simulations Fig. 4.7 was taken at a constant LO power 5.2 dBm, and the corresponding conversion loss is presented versus bias as shown in Fig. 4.10.

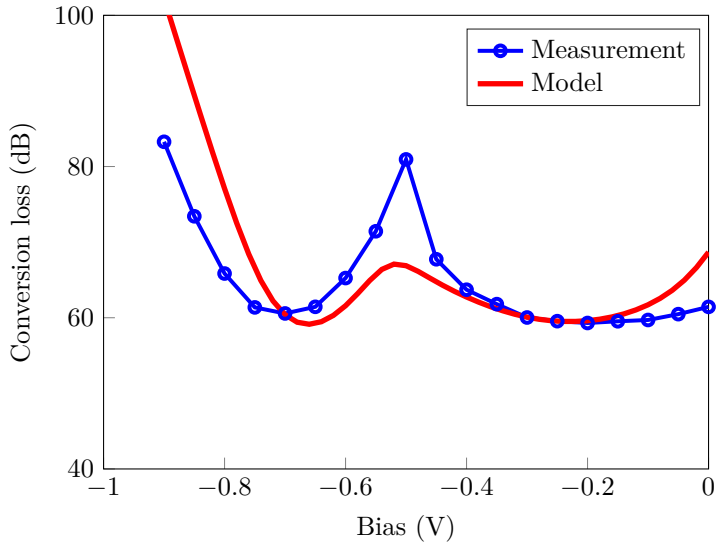

Figure 4.10: Comparison of conversion loss versus bias from measurements and simulation at a constant LO power of about 5.2 dBm.

The down-converted IF signal from the harmonic mixer is amplified by an LNA, and the signal is read out from the spectrum analyser. Fig. 4.11 shows the beat signal spectrum recorded with a resolution bandwidth of 510 kHz and a video bandwidth of 10 kHz.

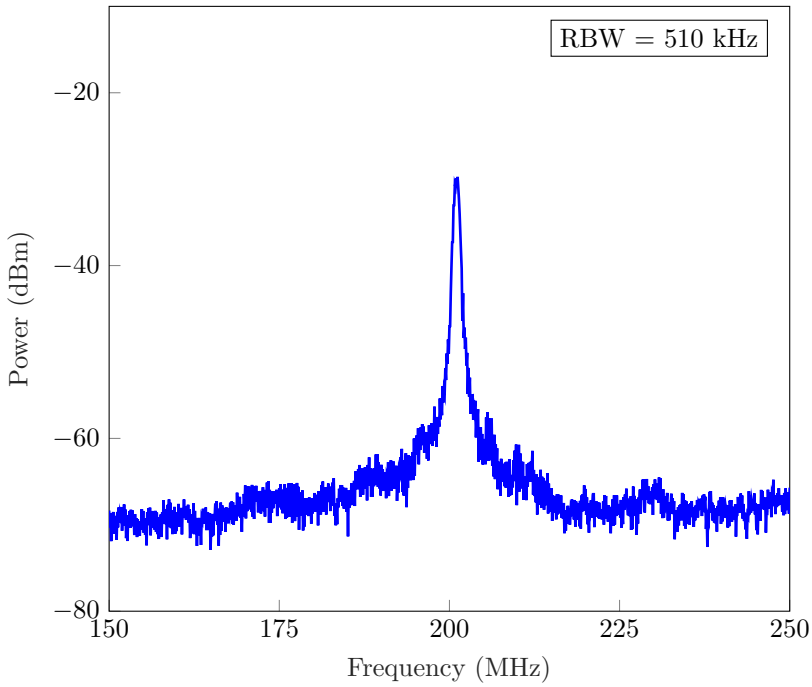

Figure 4.11: Down-converted IF signal at 200 MHz from the harmonic mixer recorded with a resolution bandwidth of 510 kHz and a video bandwidth of 10 kHz.

4.2.2 4.7-THz, ×8-harmonic mixer

The same harmonic mixer was evaluated at 4.7 THz, and using the 8^{th} harmonic of the LO signal, an IF signal at 3.7 GHz was generated. The measured RF power from 4.7-THz QCL was about −2.2 dBm, and the operating temperature of the QCL was about 50 K. At 592.3 GHz, the available LO power from the multiplier chain is about 4.6 dBm. The dc bias applied to the mixer via bias tee is varied, and the mixer conversion loss is plotted versus dc bias for a constant LO power as shown in Fig. 4.12. At 0.4 V, a conversion loss of about 76 dB was measured.

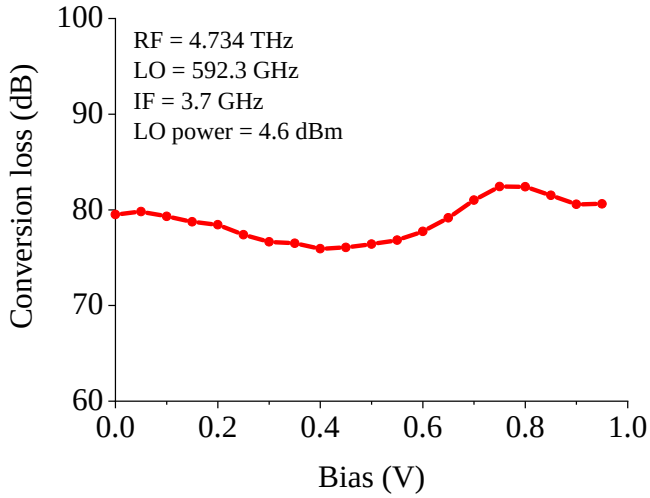

Figure 4.12: Measured conversion loss of the 4.7-THz, ×8-harmonic mixer versus dc bias at constant LO power

CHAPTER 5

Conclusion and future work

Detection of atomic and molecular spectral lines at THz frequencies is essential in atmospheric and planetary sciences. The development of QCLs has accelerated the development of THz heterodyne spectrometers above 3 THz. However, it is critical to stabilise the QCLs to resolve the fine features of the molecular spectrum.

This thesis has focused on designing and characterising a 3.5-THz, $\times$6-harmonic mixer developed for frequency stabilisation of QCLs. First, the effects of different idler terminations on mixer performance was studied. The optimum embedding impedances that offers low conversion loss were evaluated at RF and LO frequencies [Paper A]. Based on this, a 3D-EM model of the harmonic mixer was designed, and the critical parameters which influence the mixer performance were studied to evaluate the robustness of the design.

The key factors that limit the realisation of mixers at THz frequencies are higher order propagation modes and substrate loss. To circumvent this problem, the integrated mixer circuits were fabricated on a 2-μm GaAs substrate. To reduce the parasitics, Schottky contacts with an area less than 0.2 μm^2 were defined. The fabricated mixer circuits were assembled on two mixer split blocks in E-plane configuration, resulting in similar mixer performance with

a conversion loss of about 60 dB. The discrepancy between the simulations and measurements were analysed, and important conclusions are discussed in [Paper B]. One way to improve the harmonic mixer's performance is to minimise the surface roughness of the split blocks and ensure there is no gap or misalignment. [Paper C] presents an updated design with new RF/LO matching circuits and filter design. Careful geometry optimisation was carried out to reduce the spreading resistance in the buffer region, and the preliminary simulation results are promising.

In the future, it is vital to work on thermal management and to study the influence of self-heating effects on mixer performance. Another important aspect of improvement in future designs is to consider a different mixer topology. For example, anti-parallel diodes are advantageous because they suppress fundamental and odd harmonics, which can considerably improve the mixer conversion loss.

CHAPTER 6

Summary of appended papers

This chapter presents a summary of the appended papers and outlines my contribution to each paper.

Paper A

Effect of Idler Terminations on the Conversion Loss for THz Schottky Diode Harmonic Mixers

This paper presents the effect of idler terminations on conversion loss of the harmonic mixers. The optimum embedding impedances for different mixer topologies (Z- and Y-mixers) are studied.
My contribution: Writing the paper, Schottky diode modelling, analysis and simulation of harmonic mixers in different idler configurations.

Paper B

A 3.5-THz, ×6-Harmonic, Single-Ended Schottky Diode Mixer for Frequency Stabilization of Quantum-Cascade Lasers

This paper presents the design and characterisation of a 3.5-THz, ×6-harmonic mixer. Based on the theoretical study presented in [Paper A], a 3D EM design of the harmonic mixer was carried out. A sensitivity analysis was performed to evaluate the robustness of the design. The integrated harmonic mixer was realised on a 2-μm GaAs substrate and assembled on an E-plane split-block. Two mixers were assembled, and both showed similar performance [Paper C]. The harmonic mixer with 0.11 μm^2 Schottky contact area exhibited a conversion loss of about 60 dB.
My contribution: Writing the manuscript, design of the 3.5-THz, ×6-harmonic mixer, sensitivity analysis, mixer layout for circuit fabrication, CAD drawings of the mixer blocks, quartz, PCB design and assembly. DC measurements, wafer mapping, parameter extraction and RF characterisation of mixers.

Paper C

Development of Supra-THz Schottky Diode Harmonic Mixers

This paper presents RF characterisation results of the 3.5-THz harmonic mixer with a Schottky contact area of 0.14 μm^2. Also, an updated design and preliminary simulation results of a 4.7-THz, ×8-harmonic mixer is presented.
My contribution: Writing the paper, design of the 3.5-THz, ×6-harmonic and 4.7-THz, ×8-harmonic mixers.

APPENDIX

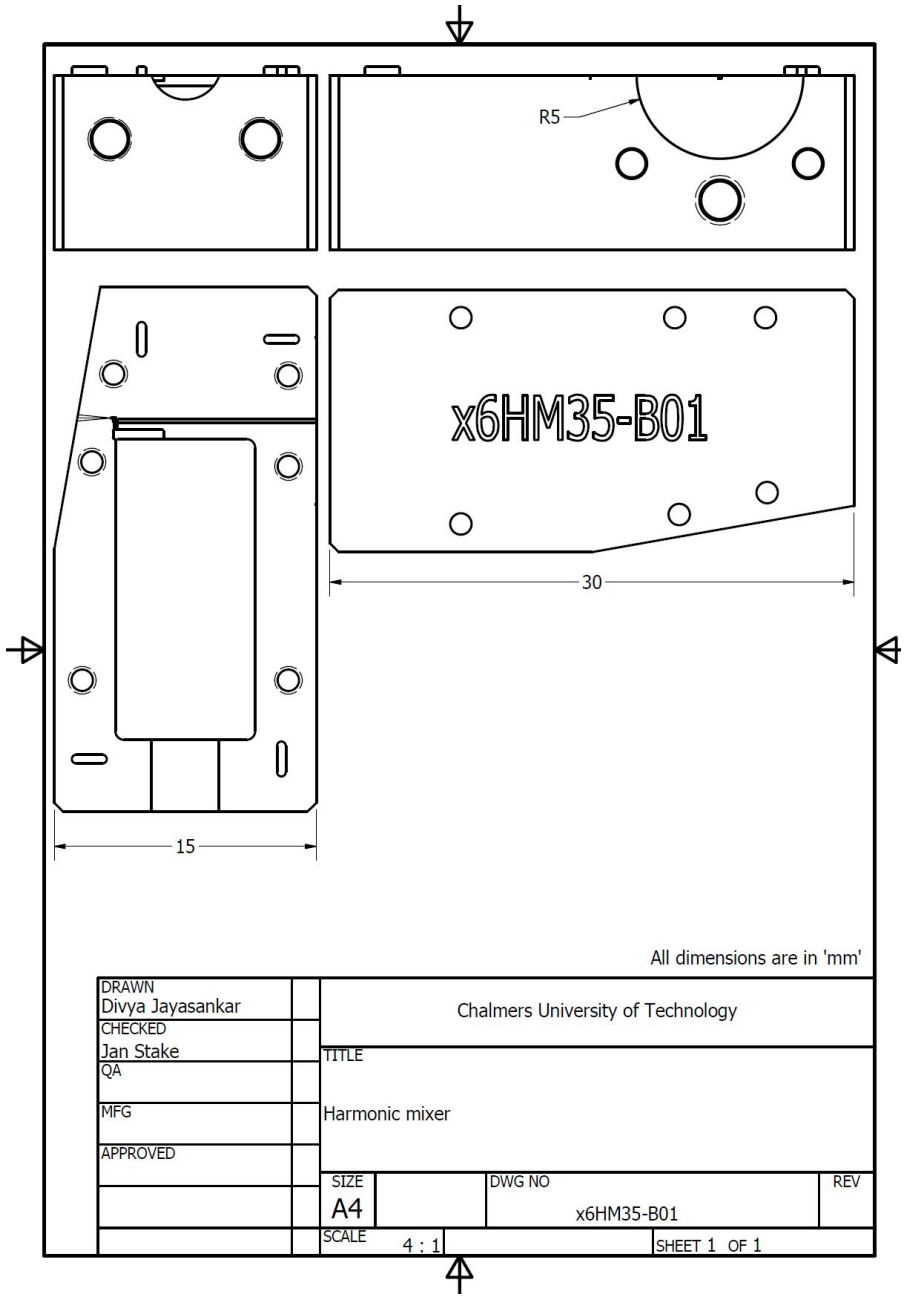

All dimensions are in 'mm'

DRAWN: Divya Jayasankar	Chalmers University of Technology
CHECKED: Jan Stake	TITLE: Harmonic mixer
QA	
MFG	
APPROVED	
SIZE: A4	DWG NO: x6HM35-B01 — REV
SCALE: 4 : 1	SHEET 1 OF 1

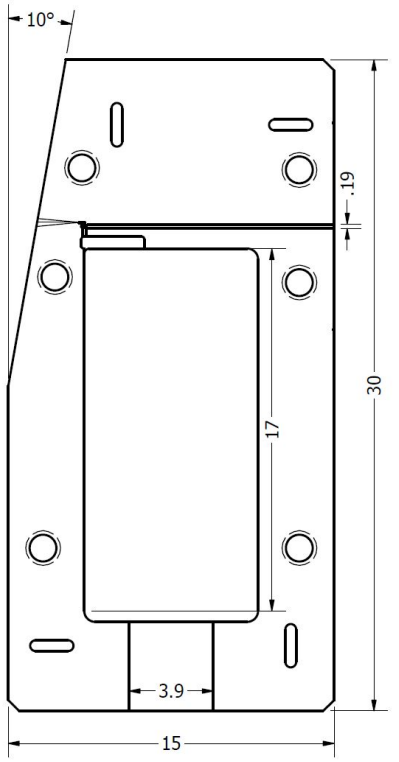

All dimensions are in 'mm'

DRAWN Divya Jayasankar		Chalmers University of Technology
CHECKED Jan Stake		TITLE
QA		
MFG		Harmonic mixer
APPROVED		
	SIZE A4	DWG NO x6HM35-B01 REV
	SCALE 5 : 1	SHEET 1 OF 1

References

[1] J. W. Waters, L. Froidevaux, R. S. Harwood, R. F. Jarnot, H. M. Pickett, W. G. Read, P. H. Siegel, R. E. Cofield, M. J. Filipiak, D. A. Flower, J. R. Holden, G. K. Lau, N. J. Livesey, G. L. Manney, H. C. Pumphrey, M. L. Santee, D. L. Wu, D. T. Cuddy, R. R. Lay, M. S. Loo, V. S. Perun, M. J. Schwartz, P. C. Stek, R. P. Thurstans, M. A. Boyles, K. M. Chandra, M. C. Chavez, G.-S. Chen, B. V. Chudasama, R. Dodge, R. A. Fuller, M. A. Girard, J. H. Jiang, Y. Jiang, B. W. Knosp, R. C. LaBelle, J. C. Lam, K. A. Lee, D. Miller, J. E. Oswald, N. C. Patel, D. M. Pukala, O. Quintero, D. M. Scaff, W. Van Snyder, M. C. Tope, P. A. Wagner, and M. J. Walch, "The Earth Observing System Microwave Limb Sounder (EOS MLS) on the Aura Satellite", *IEEE Trans. Geosci. Remote Sens.*, vol. 44, no. 5, pp. 1075–1092, May 2006. DOI: 10.1109/TGRS.2006.873771.

[2] P. H. Siegel, "THz Instruments for Space", *IEEE Trans. Antennas Propag.*, vol. 55, no. 11, pp. 2957–2965, Nov. 2007.

[3] H.-W. Hubers, "Terahertz heterodyne receivers", *IEEE Journal of Selected Topics in Quantum Electronics*, vol. 14, no. 2, pp. 378–391, 2008. DOI: 10.1109/JSTQE.2007.913964.

[4] D. Farrah, K. E. Smith, D. Ardila, C. M. Bradford, M. Dipirro, C. Ferkinhoff, J. Glenn, P. Goldsmith, D. Leisawitz, T. Nikola, N. Rangwala, S. A. Rinehart, J. Staguhn, M. Zemcov, J. Zmuidzinas, J. Bartlett, S. Carey, W. J. Fischer, J. Kamenetzky, J. Kartaltepe, M. Lacy, D. C. Lis, L. Locke, E. Lopez-Rodriguez, M. MacGregor, E. Mills, S. H. Moseley,

E. J. Murphy, A. Rhodes, M. Richter, D. Rigopoulou, D. Sanders, R. Sankrit, G. Savini, J.-D. Smith, and S. Stierwalt, "Review: Far-infrared instrumentation and technological development for the next decade", *J. Astron. Telesc. Instrumen. Syst.*, vol. 5, Apr. 2019, Art. no. 020901, DOI: 10.1117/1.jatis.5.2.020901.

[5] R. T. Boreiko and A. Betz, "Heterodyne Spectroscopy of the 63 μm O I Line in M42", *The Astrophysical Journal*, vol. 464, 1996.

[6] H. Richter, C. Buchbender, R. Güsten, R. Higgins, B. Klein, J. Stutzki, H. Wiesemeyer, and H.-W. Hübers, "Direct measurements of atomic oxygen in the mesosphere and lower thermosphere using terahertz heterodyne spectroscopy", *Commun. Earth Environment*, vol. 2, no. 1, Jan. 2021, Art. no. 19, DOI: 10.1038/s43247-020-00084-5.

[7] D. L. Wu, J.-H. Yee, E. Schlecht, I. Mehdi, J. Siles, and B. J. Drouin, "THz limb sounder (TLS) for lower thermospheric wind, oxygen density, and temperature", *Journal of Geophysical Research: Space Physics*, vol. 121, no. 7, pp. 7301–7315, Jul. 2016. DOI: 10.1002/2015ja022314.

[8] A. K. Smith, D. R. Marsh, M. G. Mlynczak, and J. C. Mast, "Temporal variations of atomic oxygen in the upper mesosphere from SABER", *Journal of Geophysical Research*, vol. 115, no. D18, Sep. 2010. DOI: 10.1029/2009jd013434.

[9] D. Gerber, B. Ellison, P. Huggard, A. Valavanis, E. Linfield, A. Davies, G. Savini, N. Bowles, S. Calcutt, M. Crook, M. Hills, S. Parkes, and S. Mills, "The ESA earth explorer 10 candidate mission LOCUS", in *UK National Earth Observation Conference*, Jun. 2018.

[10] R. Köhler, A. Tredicucci, F. Beltram, H. E. Beere, E. H. Linfield, A. G. Davies, D. A. Ritchie, R. C. Iotti, and F. Rossi, "Terahertz semiconductor-heterostructure laser", *Nature*, vol. 417, pp. 156–159, May 2002. DOI: 10.1038/417156a.

[11] B. S. Williams, "Terahertz quantum-cascade lasers", *Nature Photonics*, vol. 1, no. 9, pp. 517–525, Sep. 2007. DOI: 10.1038/nphoton.2007.166.

[12] G. Scalari, L. Ajili, J. Faist, H. Beere, E. Linfield, D. Ritchie, and G. Davies, "Far-infrared ($\lambda \simeq 87$ μm) bound-to-continuum quantum-cascade lasers operating up to 90 K", *Applied Physics Letters*, vol. 82, pp. 3165–3167, 2003.

[13] L. Schrottke, X. Lü, B. Röben, K. Biermann, T. Hagelschuer, M. Wienold, H.-W. Hübers, M. Hannemann, J. H. van Helden, J. Röpcke, and H. T. Grahn, "High-performance GaAs/AlAs terahertz quantum-cascade lasers for spectroscopic applications", *IEEE Trans. THz Sci. Technol.*, vol. 10, no. 2, pp. 133–140, Mar. 2020. DOI: 10.1109/TTHZ.2019.2957456.

[14] H.-W. Hübers, H. Richter, and M. Wienold, "High-resolution terahertz spectroscopy with quantum-cascade lasers", *Journal of Applied Physics*, vol. 125, no. 15, p. 151 401, Apr. 2019. DOI: 10.1063/1.5084105.

[15] D. Rabanus, U. U. Graf, M. Philipp, O. Ricken, J. Stutzki, B. Vowinkel, M. C. Wiedner, C. Walther, M. Fischer, and J. Faist, "Phase locking of a 1.5 terahertz quantum cascade laser and use as a local oscillator in a heterodyne HEB receiver", *Opt. Express*, vol. 17, no. 3, pp. 1159–1168, Feb. 2009. DOI: 10.1364/oe.17.001159.

[16] C. Walker, C. Kulesa, P. Bernasconi, H. Eaton, N. Rolander, C. Groppi, J. Kloosterman, T. Cottam, D. Lesser, C. Martin, A. Stark, D. Neufeld, C. Lisse, D. Hollenbach, J. Kawamura, P. Goldsmith, W. Langer, H. Yorke, J. Sterne, A. Skalare, I. Mehdi, S. Weinreb, J. Kooi, J. Stutzki, U. Graf, M. Brasse, C. Honingh, R. Simon, M. Akyilmaz, P. Puetz, and M. Wolfire, "The Stratospheric THz Observatory (STO)", in *Ground-based and Airborne Telescopes III*, L. M. Stepp, R. Gilmozzi, and H. J. Hall, Eds., International Society for Optics and Photonics, vol. 7733, SPIE, 2010, pp. 264–272. DOI: 10.1117/12.857765.

[17] U. Frisk, M. Hagström, J. Ala-Laurinaho, S. Andersson, J.-C. Berges, J.-P. Chabaud, M. Dahlgren, A. Emrich, H.-G. Florén, G. Florin, M. Fredrixon, T. Gaier, R. Haas, T. Hirvonen, Å. Hjalmarsson, B. Jakobsson, P. Jukkala, P. S. Kildal, E. Kollberg, J. Lassing, A. Lecacheux, P. Lehikoinen, A. Lehto, J. Mallat, C. Marty, D. Michet, J. Narbonne, M. Nexon, M. Olberg, A. O. H. Olofsson, G. Olofsson, A. Origné, M. Petersson, P. Piironen, R. Pons, D. Pouliquen, I. Ristorcelli, C. Rosolen, G. Rouaix, A. V. Räisänen, G. Serra, F. Sjöberg, L. Stenmark, S. Torchinsky, J. Tuovinen, C. Ullberg, E. Vinterhav, N. Wadefalk, H. Zirath, P. Zimmermann, and R. Zimmermann, "The Odin satellite", *Astronomy & Astrophysics*, vol. 402, no. 3, pp. L27–L34, Apr. 2003. DOI: 10.1051/0004-6361:20030335.

[18] S. Gulkis, M. Frerking, J. Crovisier, G. Beaudin, P. Hartogh, P. Encrenaz, T. Koch, C. Kahn, Y. Salinas, R. Nowicki, R. Irigoyen, M. Janssen, P. Stek, M. Hofstadter, M. Allen, C. Backus, L. Kamp, C. Jarchow, E. Steinmetz, A. Deschamps, J. Krieg, M. Gheudin, D. Bockelée-Morvan, N. Biver, T. Encrenaz, D. Despois, W. Ip, E. Lellouch, I. Mann, D. Muhleman, H. Rauer, P. Schloerb, and T. Spilker, "MIRO: Microwave Instrument for Rosetta Orbiter", *Space Science Reviews*, vol. 128, no. 1-4, pp. 561–597, Nov. 2006. DOI: 10.1007/s11214-006-9032-y.

[19] F. Maiwald, E. Schlecht, A. Maestrini, G. Chattopadhyay, J. C. Pearson, D. Pukala, and I. Mehdi, "Terahertz frequency multiplier chains based on planar Schottky diodes", in *Millimeter and Submillimeter Detectors for Astronomy*, T. G. Phillips and J. Zmuidzinas, Eds., International Society for Optics and Photonics, vol. 4855, SPIE, 2003, pp. 447–458. DOI: 10.1117/12.459355.

[20] A. Maestrini, L. Gatilova, J. Treuttel, Y. Jin, A. Cavanna, D. M. Melgar, T. Vacelet, A. Féret, S. Caroopen, G. Gay, F. Dauplay, J.-M. Krieg, B. Thomas, P. de Maagt, and C. Goldstein, "The 1200 GHz receiver frontend of the submillimetre wave instrument of ESA JUpiter ICy moons Explorer", in *2018 43rd International Conference on Infrared, Millimeter, and Terahertz Waves (IRMMW-THz)*, 2018, pp. 1–2. DOI: 10.1109/IRMMW-THz.2018.8509935.

[21] I. Mehdi, J. V. Siles, C. Lee, and E. Schlecht, "THz diode technology: Status, prospects, and applications", *Proc. IEEE*, vol. 105, no. 6, pp. 990–1007, Jun. 2017. DOI: 10.1109/JPROC.2017.2650235.

[22] A. L. Betz, R. T. Boreiko, B. S. Williams, S. Kumar, Q. Hu, and J. L. Reno, "Frequency and phase-lock control of a 3 THz quantum cascade laser", *Opt. Lett.*, vol. 30, no. 14, pp. 1837–1839, Jul. 2005. DOI: 10.1364/OL.30.001837.

[23] N. R. Erickson and T. M. Goyette, "Terahertz Schottky-diode balanced mixers", in *Terahertz Technology and Applications II*, K. J. Linden, L. P. Sadwick, and C. M. O'Sullivan, Eds., International Society for Optics and Photonics, vol. 7215, SPIE, 2009, pp. 41–45. DOI: 10.1117/12.807505.

[24] A. Danylov, N. Erickson, A. Light, and J. Waldman, "Phase locking of 2.324 and 2.959 terahertz quantum cascade lasers using a Schottky diode harmonic mixer", *Opt. Lett.*, vol. 40, no. 21, pp. 5090–5092, Nov. 2015. DOI: 10.1364/ol.40.005090.

[25] B. T. Bulcha, J. L. Hesler, A. Valavanis, V. Drakinskiy, J. Stake, R. Dong, J. X. Zhu, P. Dean, L. H. Li, A. G. Davies, E. H. Linfield, and N. S. Barker, "Phase locking of a 2.5 THz quantum cascade laser to a microwave reference using THz Schottky mixer", in *2015 40th Int. Conf. on Infrared, Millimeter, and Terahertz waves (IRMMW-THz)*, 2015, pp. 1–2. DOI: 10.1109/IRMMW-THz.2015.7327689.

[26] B. T. Bulcha, J. L. Hesler, V. Drakinskiy, J. Stake, A. Valavanis, P. Dean, L. H. Li, and N. S. Barker, "Design and characterization of 1.8–3.2 THz Schottky-based harmonic mixers", *IEEE Trans. THz Sci. Technol.*, vol. 6, no. 5, pp. 737–746, Sep. 2016. DOI: 10.1109/TTHZ.2016.2576686.

[27] S. Maas, *The RF and Microwave Circuit Design Cookbook*, ser. Artech House Mobile Communicat. Artech House, 1998.

[28] K. Braun, "On the current conduction in metal sulphides (title translated from german into english", *Ann. Phys. chem.*, vol. 153, 1874. DOI: 10.1002/andp.18752291207.

[29] E. EASTWOOD, "Marconi: His wireless telegraphy and the modern world", *Journal of the Royal Society of Arts*, vol. 122, no. 5217, pp. 599–611, 1974.

[30] J. Bose, "Detector for electrical disturbances patent", *Proceedings of the IEEE*, vol. 86, no. 1, pp. 229–234, 1998. DOI: 10.1109/JPROC.1998.658774.

[31] W. Schottky, "Halbleitertheorie der sperrschicht", *Naturwissenschaften*, vol. 26, no. 52, pp. 843–843, Dec. 1938. DOI: 10.1007/BF01774216.

[32] V. Rideout, "A review of the theory, technology and applications of metal-semiconductor rectifiers", *Thin Solid Films*, vol. 48, no. 3, pp. 261–291, Feb. 1978. DOI: 10.1016/0040-6090(78)90007-x.

[33] A. M. Cowley and S. M. Sze, "Surface states and barrier height of metal-semiconductor systems", *Journal of Applied Physics*, vol. 36, no. 10, pp. 3212–3220, Oct. 1965. DOI: 10.1063/1.1702952.

[34] W. Mönch, "On the physics of metal-semiconductor interfaces", *Reports on Progress in Physics*, vol. 53, no. 3, pp. 221–278, Mar. 1990. DOI: 10.1088/0034-4885/53/3/001.

[35] D. Young and J. Irvin, "Millimeter frequency conversion using Au-n-type GaAs Schottky barrier epitaxial diodes with a novel contacting technique", *Proceedings of the IEEE*, vol. 53, no. 12, pp. 2130–2131, 1965. DOI: 10.1109/PROC.1965.4511.

[36] V. Rideout, "A review of the theory and technology for ohmic contacts to group III-V compound semiconductors", *Solid-State Electronics*, vol. 18, no. 6, pp. 541–550, Jun. 1975. DOI: 10.1016/0038-1101(75)90031-3.

[37] E. H. Rhoderick, "The physics of Schottky barriers", *J. Phys. D: Appl. Phys*, vol. 3, no. 8, pp. 1153–1167, 1970.

[38] P. Penfield and R. Rafuse, *Varactor applications*. MIT press, 1962.

[39] A. Maestrini, B. Thomas, H. Wang, C. Jung, J. Treuttel, Y. Jin, G. Chattopadhyay, I. Mehdi, and G. Beaudin, "Schottky diode-based terahertz frequency multipliers and mixers", *Comptes Rendus Physique*, vol. 11, no. 7-8, pp. 480–495, Aug. 2010. DOI: 10.1016/j.crhy.2010.05.002.

[40] S. Adachi, *Properties of group-IV, III-V and II-VI semiconductors*. John Wiley and Sons, 2005.

[41] E. D. Palik, "Gallium arsenide (GaAs)", in *Handbook of Optical Constants of Solids*, E. D. Palik, Ed., Boston, MA, USA: Academic Press, 1985, pp. 429–443. DOI: 10.1016/B978-0-08-054721-3.50020-4.

[42] M. Sotoodeh, A. H. Khalid, and A. A. Rezazadeh, "Empirical low-field mobility model for III-V compounds applicable in device simulation codes", *Journal of Applied Physics*, vol. 87, no. 6, pp. 2890–2900, 2000. DOI: 10.1063/1.372274.

[43] O. H. Richardson, "The emission of electricity from hot bodies", *Nature*, vol. 98, no. 2452, pp. 146–146, Oct. 1916. DOI: 10.1038/098146a0.

[44] H. A. Bethe, "Theory of the boundary layer of crystal rectifiers", 1991.

[45] M. Missous, E. H. Rhoderick, D. A. Woolf, and S. P. Wilkes, "On the Richardson constant of intimate metal-GaAs Schottky barriers", *Semiconductor Science and Technology*, vol. 7, no. 2, pp. 218–221, Feb. 1992. DOI: 10.1088/0268-1242/7/2/007.

[46] S.Maas, *Nonlinear microwave and RF circuits. Artech House, Inc.* 2003.

[47] J. Louhi, "The capacitance of a small circular Schottky diode for submillimeter wavelengths", *IEEE Microw. Guided Wave Lett.*, vol. 4, no. 4, pp. 107–108, Apr. 1994. DOI: 10.1109/75.282574.

[48] D. Moro-Melgar, A. Maestrini, J. Treuttel, L. Gatilova, T. González, B. G. Vasallo, and J. Mateos, "Monte carlo study of 2-D capacitance fringing effects in GaAs planar Schottky diodes", *IEEE Transactions on Electron Devices*, vol. 63, no. 10, pp. 3900–3907, 2016. DOI: 10.1109/TED.2016.2601341.

[49] L. E. Dickens, "Spreading resistance as a function of frequency", *IEEE Trans. Microw. Theory Techn.*, vol. 15, no. 2, pp. 101–109, Feb. 1967. DOI: 10.1109/TMTT.1967.1126383.

[50] H. Wheeler, "Formulas for the skin effect", *Proceedings of the IRE*, vol. 30, no. 9, pp. 412–424, 1942. DOI: 10.1109/JRPROC.1942.232015.

[51] A. Y. Tang, P. Sobis, H. Zhao, V. Drakinskiy, T. Bryllert, and J. Stake, "Analysis of the high frequency spreading resistance for surface channel planar Schottky diodes", in *35th International Conference on Infrared, Millimeter, and Terahertz Waves*, 2010, pp. 1–2. DOI: 10.1109/ICIMW.2010.5612850.

[52] K. Bhaumik, B. Gelmont, R. Mattauch, and M. Shur, "Series impedance of GaAs planar schottky diodes operated to 500 GHz", *IEEE Transactions on Microwave Theory and Techniques*, vol. 40, no. 5, pp. 880–885, 1992. DOI: 10.1109/22.137393.

[53] N. Alijabbari, M. F. Bauwens, and R. M. Weikle, "Design and Characterization of Integrated Submillimeter-Wave Quasi-Vertical Schottky Diodes", *IEEE Trans. THz Sci. Technol.*, vol. 5, no. 1, pp. 73–80, Jan. 2015. DOI: 10.1109/TTHZ.2014.2361434.

[54] R. Cox and H. Strack, "Ohmic contacts for GaAs devices", *Solid-State Electronics*, vol. 10, no. 12, pp. 1213–1218, Dec. 1967. DOI: 10.1016/0038-1101(67)90063-9.

[55] H. Murrmann and D. Widmann, "Current crowding on metal contacts to planar devices", *IEEE Transactions on Electron Devices*, vol. 16, no. 12, pp. 1022–1024, 1969. DOI: 10.1109/T-ED.1969.16904.

[56] K. S. Champlin and G. Eisenstein, "Cutoff frequency of submillimeter Schottky-barrier diodes", *IEEE Trans. Microw. Theory Techn.*, vol. 26, no. 1, pp. 31–34, Jan. 1978. DOI: 10.1109/TMTT.1978.1129302.

[57] N. Wadefalk, A. Mellberg, I. Angelov, M. Barsky, S. Bui, E. Choumas, R. Grundbacher, E. Kollberg, R. Lai, N. Rorsman, P. Starski, J. Stenarson, D. Streit, and H. Zirath, "Cryogenic wide-band ultra-low-noise IF amplifiers operating at ultra-low DC power", *IEEE Transactions on Microwave Theory and Techniques*, vol. 51, no. 6, pp. 1705–1711, 2003. DOI: 10.1109/TMTT.2003.812570.

[58] A. A. M. Saleh, "Theory of resistive mixers", PhD thesis, Dept. Elect. Eng., MIT, Cambridge, MA, USA, 1970.

[59] K. Yhland, "Simplified analysis of resistive mixers", *IEEE Microwave and Wireless Components Letters*, vol. 17, no. 8, pp. 604–606, 2007. DOI: 10.1109/LMWC.2007.901785.

[60] P. K. Tien, "Parametric amplification and frequency mixing in propagating circuits", *Journal of Applied Physics*, vol. 29, no. 9, pp. 1347–1357, Sep. 1958. DOI: 10.1063/1.1723440.

[61] R. Bauer, M. Cohn, J. Cotton, and R. Packard, "Millimeter wave semiconductor diode detectors, mixers, and frequency multipliers", *Proceedings of the IEEE*, vol. 54, no. 4, pp. 595–605, 1966. DOI: 10.1109/PROC.1966.4779.

[62] A. Hammar, P. Sobis, V. Drakinskiy, A. Emrich, N. Wadefalk, J. Schleeh, and J. Stake, "Low noise 874 GHz receivers for the international submillimetre airborne radiometer (ISMAR)", *Review of Scientific Instruments*, vol. 89, no. 5, p. 055 104, May 2018. DOI: 10.1063/1.5017583.

[63] M. Cohn, J. Degenford, and B. Newman, "Harmonic mixing with an antiparallel diode pair", *IEEE Transactions on Microwave Theory and Techniques*, vol. 23, no. 8, pp. 667–673, 1975. DOI: 10.1109/TMTT.1975.1128646.

[64] J. V. Siles, K. B. Cooper, C. Lee, R. H. Lin, G. Chattopadhyay, and I. Mehdi, "A new generation of room-temperature frequency-multiplied sources with up to 10x higher output power in the 160-GHz–1.6-THz range", *IEEE Transactions on Terahertz Science and Technology*, vol. 8, no. 6, pp. 596–604, 2018. DOI: 10.1109/TTHZ.2018.2876620.

[65] A. Kelly, "Fundamental limits on conversion loss of double sideband resistive mixers", *IEEE Transactions on Microwave Theory and Techniques*, vol. 25, no. 11, pp. 867–869, 1977. DOI: 10.1109/TMTT.1977.1129233.

[66] A. Y. Tang, E. Schlecht, R. Lin, G. Chattopadhyay, C. Lee, J. Gill, I. Mehdi, and J. Stake, "Electro-thermal model for multi-anode Schottky diode multipliers", *IEEE Trans. THz Sci. Technol.*, vol. 2, no. 3, pp. 290–298, May 2012. DOI: 10.1109/TTHZ.2012.2189913.

[67] J. Johnson, "Thermal agitation of electricity in conductors", *Phys. Rev.*, vol. 32, no. 1, pp. 97–109, 1928.

[68] H. Nyquist, "Thermal agitation of electric charge in conductors", *Phy. Rev.*, vol. 32, no. 1, pp. 110–113, 1928.

[69] A. V. Der Ziel, "Theory of shot noise in junction diodes and junction transistors", *Proceedings of the IRE*, vol. 43, no. 11, pp. 1639–1646, 1955. DOI: 10.1109/JRPROC.1955.277990.

[70] H. Zirath, "High-frequency noise and current-voltage characteristics of mm-wave platinum $n - n + -$GaAs schottky barrier diodes", vol. 60, no. 4, pp. 1399–1407, Aug. 1986. DOI: 10.1063/1.337317.

[71] E. T. Schlecht, J. J. Gill, R. H. Lin, R. J. Dengler, and I. Mehdi, "A 520–590 GHz Crossbar Balanced Fundamental Schottky Mixer", *IEEE Microwave and Wireless Components Letters*, vol. 20, no. 7, pp. 387–389, 2010. DOI: 10.1109/LMWC.2010.2049432.

[72] P. J. Sobis, A. Emrich, and J. Stake, "A Low VSWR 2SB Schottky Receiver", *IEEE Transactions on Terahertz Science and Technology*, vol. 1, no. 2, pp. 403–411, 2011. DOI: 10.1109/TTHZ.2011.2166176.

[73] J. Treuttel, L. Gatilova, A. Maestrini, D. Moro-Melgar, F. Yang, F. Tamazouzt, T. Vacelet, Y. Jin, A. Cavanna, J. Matéos, A. Féret, C. Chaumont, and C. Goldstein, "A 520–620-GHz Schottky Receiver Front-End for Planetary Science and Remote Sensing With 1070 K–1500 K DSB Noise Temperature at Room Temperature", *IEEE Transactions on Terahertz Science and Technology*, vol. 6, no. 1, pp. 148–155, 2016. DOI: 10.1109/TTHZ.2015.2496421.

[74] Pütz, P., Honingh, C. E., Jacobs, K., Justen, M., Schultz, M., and Stutzki, J., "Terahertz hot electron bolometer waveguide mixers for GREAT", *A&A*, vol. 542, p. L2, 2012. DOI: 10.1051/0004-6361/201218916.

[75] J. L. Hesler, H. Xu, A. Brissette, and W. L. Bishop, "Development and characterization of THz planar Schottky diode mixers and detectors", in *2008 19th Int. Sym. on Space Terahertz Technology*, Groningen, 2008.

[76] "IEEE Standard for Rectangular Metallic Waveguides and Their Interfaces for Frequencies of 110 GHz and Above–Part 1: Frequency Bands and Waveguide Dimensions", *IEEE Std 1785.1-2012*, pp. 1–22, Mar. 2013. DOI: 10.1109/IEEESTD.2013.6471987.

[77] E. Carlson, M. Schneider, and T. McMaster, "Subharmonically pumped millimeter-wave mixers", *IEEE Transactions on Microwave Theory and Techniques*, vol. 26, no. 10, pp. 706–715, 1978. DOI: 10.1109/TMTT.1978.1129474.

[78] W. Bishop, E. Meiburg, R. Mattauch, T. Crowe, and L. Poli, "A micron-thickness, planar Schottky diode chip for terahertz applications with theoretical minimum parasitic capacitance", in *IEEE International Digest on Microwave Symposium*, 1990, 1305–1308 vol.3. DOI: 10.1109/MWSYM.1990.99818.

[79] P. H. Siegel, R. P. Smith, M. C. Graidis, and S. C. Martin, "2.5-THz GaAs monolithic membrane-diode mixer", *IEEE Trans. Microw. Theory Techn.*, vol. 47, no. 5, pp. 596–604, May 1999. DOI: 10.1109/22.763161.

[80] V. Drakinskiy, P. Sobis, H. Zhao, T. Bryllert, and J. Stake, "Terahertz GaAs Schottky diode mixer and multiplier MIC's based on e-beam technology", in *2013 International Conference on Indium Phosphide and Related Materials (IPRM)*, May 2013, pp. 1–2. DOI: 10.1109/ICIPRM.2013.6562606.

[81] D. Jayasankar, J. Stake, and P. Sobis, "Effect of idler terminations on the conversion loss for THz Schottky diode harmonic mixers", *2019 44th Int. Conf. on Infrared, Millimeter, and Terahertz waves (IRMMW-THz)*, 2019, Paris, pp. 1–2. DOI: 10.1109/IRMMW-THz.2019.8873938.

[82] R. Wylde, "Millimetre-wave gaussian beam-mode optics and corrugated feed horns", English, *IEEE Proceedings in Microwaves, Optics and Antennas*, vol. 131, 258–262(4), 4 Aug. 1984.

[83] P. Potter, "A new horn antenna with suppressed sidelobes and equal beamwidths", *Microwave Journal*, p. 71, 1963.

[84] K. K. Davis, J. L. Kloosterman, C. Groppi, J. H. Kawamura, and M. Underhill, "Micromachined integrated waveguide transformers in THz Pickett–Potter feedhorn blocks", *IEEE Transactions on Terahertz Science and Technology*, vol. 7, no. 6, pp. 649–656, 2017. DOI: 10.1109/TTHZ.2017.2760103.

[85] A. Love, "The diagonal horn antenna", *Microwave Journal*, pp. 117–122, 1962.

[86] J. F. Johansson and N. D. Whyborn, "The diagonal horn as a submillimeter wave antenna", *IEEE Trans. Microw. Theory Techn.*, vol. 40, no. 5, pp. 795–800, May 1992. DOI: 10.1109/22.137380.

[87] D. Pozar, *Microwave Engineering, 4th Edition*. Wiley, 2011.

[88] P. J. Sobis, N. Wadefalk, A. Emrich, and J. Stake, "A Broadband, Low Noise, Integrated 340 GHz Schottky Diode Receiver", *IEEE Microwave and Wireless Components Letters*, vol. 22, no. 7, pp. 366–368, 2012. DOI: 10.1109/LMWC.2012.2202280.

[89] E. D. Smith, F. Szidarovszky, W. J. Karnavas, and A. T. Bahill, "Sensitivity analysis, a powerful system validation technique", *Open Cybern. Syst. J.*, vol. 2, pp. 39–56, Jan. 2008. DOI: 10.2174/1874110x00802010039.

[90] D. Jayasankar, V. Drakinskiy, P. Sobis, and J. Stake, "Development of supra-THz Schottky diode harmonic mixers", pp. 1–2, 2021. DOI: 10.1109/IRMMW-THz50926.2021.9567206.

[91] H. Richter *et al.*, "Phase locking of 3.5-THz and 4.7-THz quantum-cascade lasers using a Schottky diode harmonic mixer", *presented at the 2021 46th Int. Conf. on Infrared, Millimeter, and Terahertz waves (IRMMW-THz)*, Aug. 2021, Chengdu, pp. 1–2. DOI: 10.1109/IRMMW-THz50926.2021.9566876.

[92] J. Stake, L. Dillner, S. Jones, C. Mann, J. Thornton, J. Jones, W. Bishop, and E. Kollberg, "Effects of self-heating on planar heterostructure barrier varactor diodes", *IEEE Transactions on Electron Devices*, vol. 45, no. 11, pp. 2298–2303, 1998. DOI: 10.1109/16.726644.

[93] S. K. Cheung and N. W. Cheung, "Extraction of Schottky diode parameters from forward current-voltage characteristics", *Applied Physics Letters*, vol. 49, no. 2, pp. 85–87, Jul. 1986. DOI: 10.1063/1.97359.

[94] R. Feinäugle, H.-W. Hübers, H. P. Röser, and J. L. Hesler, "On the effect of IF power nulls in Schottky diode harmonic mixers", *IEEE Trans. Microw. Theory Techn.*, vol. 50, no. 1, pp. 134–142, Jan. 2002. DOI: 10.1109/22.981257.